

Propulsion performance of tandem flapping foils with chordwise prescribed deflection from linear potential theory

J. Alaminos-Quesada  and R. Fernandez-Feria 

Fluid Mechanics Group, University of Málaga, Dr Ortiz Ramos s/n, 29071 Málaga, Spain



(Received 2 June 2020; accepted 23 November 2020; published 22 January 2021)

The effect of prescribed flexural deflection on the propulsive performance of tandem-arranged flapping foils is analyzed by using the vortex impulse formulation in the limit of two-dimensional, linear potential flow theory. Analytical expressions are given for a general configuration of tandem foils undergoing a quadratic flexural deflection coupled with heaving and pitching motions about arbitrary pitching and deflection axes, although quantitative results are focused to the cases pivoting about their leading edges. Flexural deflection may augment not only the thrust and the propulsive efficiency of the individual foils in relation to an otherwise identical rigid-foil configuration, it also modifies the wake behind the front foil, changing the wake interaction with the trailing foil and, consequently, modifying the tandem propulsive performance. The effect of the upstream wake on the thrust force of the trailing foil is analyzed by using the vorticity distributions obtained analytically. Patterns of propulsive performance enhancement in both the spacing-frequency and the spacing-phase shift planes are analyzed and discussed in relation to previous available experimental and numerical results. The present theoretical results provide some new insights for the design of small aerial or aquatic vehicles using biomimetic tandem propulsors.

DOI: [10.1103/PhysRevFluids.6.013102](https://doi.org/10.1103/PhysRevFluids.6.013102)

I. INTRODUCTION

It is well known that the wake-foil interactions between flapping foils in tandem arrangement may produce propulsive benefits which have been exploited by animals to improve their locomotion capabilities, especially by dragonflies, among other living and extinct insect species [1–3], but also by fish, combining the dorsal-caudal fin configuration [4,5], by bird flocks and fish schools [6,7], and even by extinct aquatic animals [8]. A large number of works have been published about these unsteady aerodynamic interactions between adjacent flapping foils, both to try to understand the physical mechanisms leading to the propulsion improvement and to characterize the optimal kinematics and geometric configurations generating these propulsive benefits, some of them focused on the application to the design of biomimetic aerial and aquatic vehicles. These investigations have been based on complex two-dimensional, or three-dimensional, numerical simulations of tandem flapping rigid foils in forward flight [9–17], or on sophisticated experimental techniques [3,4,12,18–27], and just a few of them making use of some theoretical, simplified approach, especially based on two-dimensional, linear potential flow theory [28–30].

Although the validity of the last mentioned theoretical approach is limited to high Reynolds number flow and to small flapping amplitudes, so that the flow does not separate and the wakes remain almost flat, it provides useful insight into the combined effect of the huge number of geometric and kinematic parameters on the propulsive performance of the tandem flapping foils. This insight is valuable in spite of the fact that some interesting configurations in terms of thrust and propulsive efficiency are often found in the range of high amplitudes where the linearized theory

fails. For instance, using two-dimensional, potential flow theory, Bosch [28] showed that a lifting surface at rest located behind a pitching or a heaving foil considerably improves the propulsive efficiency of the resulting tandem arrangement, almost independently of the reduced frequency and the backward position of the trailing surface. This theory explained a previous experimental finding by Schmidt [31] that a stationary wing placed in the oscillatory wake of a flapping wing could generate additional thrust by recovering some of the energy released in the wake of the flapping airfoil. Later numerical simulations at high Reynolds numbers, without considering viscous effects [9], corroborated the theoretical results, finding that with appropriate selection of the frequency, amplitude, and separation of the leading foil, the tandem propulsive efficiency could be augmented more than 40% in relation to a single airfoil. However, later experiments and numerical simulations at low to moderate Reynolds numbers [13,18], although in qualitative agreement with the inviscid results, showed that this benefit was greatly outweighed by the effect of viscous drag.

Using potential flow theory for two heaving foils in tandem configuration, Lan [29] showed that the maximum thrust can be generated with maximum power efficiency if the trailing foil flaps in advance to the front one by 90° to 180° , depending on the reduced frequency and the foil separation. For two pitching foils this author found that, for a reduced frequency of 0.75 and a separation between half and one chord length, the best propulsive efficiency is obtained when pitch leads heave by about 90° , while the maximum thrust is obtained for 45° . These results are again in qualitative agreement with later experimental studies, where it was shown that aerodynamic power requirement can be reduced up to 22% compared with a pair of isolated wings when the trailing wing leads the front one by about 90° in hovering flight [20,32], while the maximum thrust and propulsive efficiency in wind tunnel experiments were observed at phase angles from 0° to 50° [19], depending on the reduced frequency and the foil spacing, in any case when the trailing foil leads the flapping motion.

More recently, a general analytical formulation of the aerodynamics performance of two heaving and pitching rigid foils in tandem configuration, based on the linearized potential flow theory, has been developed in Ref. [30], with the thrust forces computed following the vortex impulse theory [33]. These theoretical results showed that the thrust and the propulsive efficiency are greatly enhanced in relation to those of an isolated flapping foil when certain combinations of the reduced frequency and the dimensionless separation between the foils are used, that depend on the phasing between their oscillatory motions. For heaving foils, these combinations, or aerodynamic amplification modes, correspond to specific values of the so-called schooling number, in very good agreement with experimental results by Ramanarivo *et al.* [23] and by Newbolt *et al.* [26].

All these works are for rigid foils in a tandem arrangement. Flexibility of flapping wings and fins is known to greatly enhance the propulsive performance of natural fliers and swimmers. For single foils, its effect on the thrust force and the propulsive efficiency has been extensively analyzed [34–40]. For tandem arrangements of flapping foils only a few recent works based on two-dimensional flow simulations are available, either assuming potential flow [41], or by solving the full Navier-Stokes equations coupled with the flexible foil dynamics [42–45]. As already mentioned, owing to the complexity of the numerical simulations, especially for the moderate Reynolds numbers of interest in biomimetic aerial or aquatic vehicles, only very limited ranges of just a few of the many parameters governing the problem can be realistically analyzed. For this reason it is of interest to dispose of some analytical foresight from the two-dimensional, linear potential flow theory, even if the results are limited to high Reynolds numbers without flow separation, i.e., for small flapping amplitudes, which on many occasions of physical interest are far from the optimal propulsion configurations. This is the aim of the present work: to extend the analytical results of Ref. [30] to tandem flapping foils with prescribed chordwise deflection, so that the propulsive benefits of flexibility in these tandem arrangements may be characterized over an ample range of parameters. To that end we have at our disposal the recent analytical results for the propulsive performance of a single flexible foil undergoing a wide class of prescribed undulating and flexural motions, obtained from the impulse theory in the linear potential flow limit [46]. We shall consider the case in which a prescribed quadratic deflection of small amplitude is added to the pitching and heaving motions of each foil, so that the effect of a flexural motion of small amplitude on

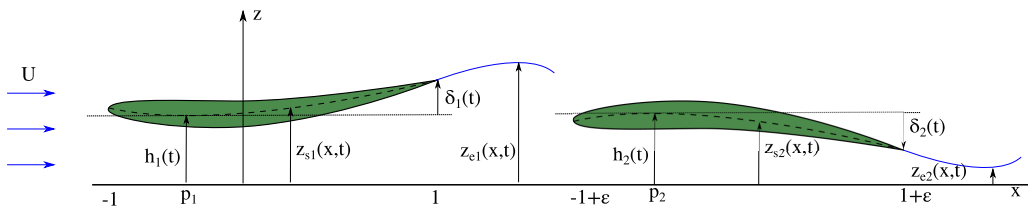


FIG. 1. Schematic of the oscillating airfoils for heaving and flexural motions (dimensionless).

the propulsive performance of the tandem arrangement is characterized with a lowest-order model. Although we sometimes use the word “flexible” for short, we do not consider here the fluid-structure interaction.

The structure of the paper is as follows: The problem is formulated in Sec. II, with the results for the general expressions of the vorticity distributions, thrust, input power, and propulsive efficiency given in Sec. III. To reduce the extent of this last section, we refer to Ref. [30] for some common derivations and relegate some of the analytical expressions to Appendixes and the Supplemental Material [47]. Section IV summarizes the validation of the model, while Sec. V analyzes the effect of the upstream wake on the thrust of the trailing foil using the vorticity distributions derived analytically in Sec. III. Section VI reports and discusses a selection of results for two cases where the effect of flexibility on the propulsive performance of tandem flapping foils is more interesting and for which the results of the present theory, but for rigid foils, compare favorably with previous experimental results, so that one may see how flexural deflection improves further the propulsive performance of the tandem arrangement. Finally, the main conclusions are summarized in Sec. VII.

II. FORMULATION OF THE PROBLEM

We consider the two-dimensional, incompressible and inviscid flow over two pitching and heaving thin airfoils of chord length c that move with constant speed U along the negative x axis. Superimposed on these motions, each foil undergoes a quadratic flexural (or deflection) motion. All these heaving, pitching, and deflection motions, which are prescribed oscillatory motions given below, have very small amplitudes compared with c , so that the airfoils, and every point of each trail of vortices that they leave behind, may be considered to be on a horizontal plane ($z = 0$) to a first approximation.

We use dimensionless variables, with all the lengths scaled with the half-chord $c/2$ and the time t scaled with $c/(2U)$. Thus, the front foil extends from $x = -1$ to $x = 1$ in a reference frame translating with it at speed U along the x axis (see Fig. 1). The trailing foil is separated by a horizontal dimensionless distance d from the trailing edge of the front foil, i.e., $\varepsilon = d + 2$ from the leading edge of the front foil, so that it is located between $x = -1 + \varepsilon$ and $x = 1 + \varepsilon$.

In this reference frame, the dimensionless vertical displacement of the mean-camber line of each foil i , with $i = 1$ and 2 for the front and back foil, respectively, is given by

$$z_{si}(x, t) = h_i(t) - (x - \varepsilon_i - a_i)\alpha_i(t) + (x - \varepsilon_i - p_i)^2\delta_i(t), \quad -1 + \varepsilon_i \leq x \leq 1 + \varepsilon_i, \quad (1)$$

with $\varepsilon_1 = 0$, $\varepsilon_2 = \varepsilon$, and

$$h_i(t) = \text{Re}[H_{0i}e^{i(kt)}], \quad \alpha_i(t) = \text{Re}[\alpha_{0i}e^{i(kt)}], \quad \delta_i(t) = \text{Re}[\delta_{0i}e^{i(kt)}]. \quad (2)$$

In these expressions Re means real part, $k = \omega c/(2U)$ is the reduced frequency associated with the frequency ω of the harmonic motion, with nondimensional period $T = 2\pi/k$, which consists of a heaving displacement $h_i(t)$, a pitching rotation $\alpha_i(t)$ pivoting at $x = a_i$, and a quadratic deflection motion $\delta_i(t)$ pivoting at $x = p_i$ (note that $a_i = -1$ and $p_i = -1$ correspond to the leading edge of each foil i , while $a_i = 1$ and $p_i = 1$ correspond to the trailing edge). The amplitudes H_{0i} , α_{0i} , and δ_{0i} are, in general, complex to allow for phase shifts between the different harmonic motions, satisfying

$|H_{0i}| \ll 1$, $|\alpha_{0i}| \ll 1$, and $|\delta_{0i}| \ll 1$. For simplicity we select $H_{01} = h_{01}$ real and

$$H_{02} = h_{02}e^{i\varphi}, \quad \alpha_{0i} = a_{0i}e^{i(\phi_i+\varphi)}, \quad \delta_{0i} = \frac{d_{mi}}{(1-p_i)^2}e^{i(\psi_i+\varphi)}, \quad (3)$$

where φ is the phase shift between the heaving motions of each foil, ϕ_i is the phase shift between the heaving and pitching motions of the foil i , ψ_i are the phase shift between the heaving and deflection motions, a_{0i} is the pitch amplitude of the foil i , and d_{mi} is the amplitude of the flexure component of the motion of foil i at its trailing edge. In what follows we shall work with the complex expressions knowing that we have to take the real part of the results.

To facilitate the computations, the vertical displacement of each foil i is written as

$$z_{si}(x, t) = \mathcal{F}_i(t) + \mathcal{E}_i(t)(x - \varepsilon_i) + \mathcal{D}_i(t)(x - \varepsilon_i)^2, \quad (4)$$

where the functions $\mathcal{F}_i(t)$, $\mathcal{E}_i(t)$, and $\mathcal{D}_i(t)$ are

$$\mathcal{F}_i(t) = h_i(t) + a_i\alpha_i(t) + p_i^2\delta_i(t), \quad \mathcal{E}_i(t) = -\alpha_i(t) - 2p_i\delta_i(t), \quad \mathcal{D}_i(t) = \delta_i(t). \quad (5)$$

The corresponding dimensionless vertical velocity of the mean-camber line of each foil can be written as

$$v_{0i}(x, t) = \mathcal{U}_i(t) + \mathcal{V}_i(t)(x - \varepsilon_i) + \dot{\mathcal{D}}_i(t)(x - \varepsilon_i)^2, \quad (6)$$

with

$$\mathcal{U}_i(t) = \dot{\mathcal{F}}_i(t) + \mathcal{E}_i(t), \quad \mathcal{V}_i(t) = \dot{\mathcal{E}}_i(t) + 2\mathcal{D}_i(t), \quad (7)$$

where a dot denotes a time derivative.

III. GENERAL EXPRESSIONS FOR THE LIFT, THRUST, MOMENT, AND INPUT POWER

A. Vorticity distributions and time-dependent coefficients

The normal velocities (6) are used to compute the vorticity distributions on both airfoils and along their wakes considering all the mutual interactions, as done in Ref. [30] for the case of two rigid airfoils in tandem configuration, but now with the additional terms coming from the quadratic flexural motions. We refer to this reference for the details of the computations, taking also into account that most of the new integrals involving the quadratic deflection terms are reported [46] for the case of a single airfoil (but now in the absence of undulatory motion, i.e., with $\mathbf{b} = 0$). The resulting vorticity distribution and the corresponding circulation around each airfoil are the following:

$$\varpi_{0i}(x, t) = \sqrt{\frac{1-x+\varepsilon_i}{1+x-\varepsilon_i}} \left\{ \frac{\Gamma_{0i}}{\pi} - [1+2(x-\varepsilon_i)]\mathcal{V}_i - 2(x-\varepsilon_i)[1+(x-\varepsilon_i)]\dot{\mathcal{D}}_i \right\}, \quad (8)$$

$$\Gamma_{0i}(t) = -\pi[2\mathcal{U}_i(t) + \mathcal{V}_i(t) + \dot{\mathcal{D}}_i(t)]. \quad (9)$$

The vorticity distribution along each wake, ϖ_{ei} , $i = 1, 2$, can be written as

$$\varpi_{e1} = \left\{ \frac{F_a(k, \varepsilon)}{\mathbf{a}(k)}\Gamma_{01}(t) + \frac{F_b(k, \varepsilon)}{\mathbf{a}(k)}[\Gamma_{02}(t) + \Gamma_{12}(t)] \right\} e^{-ik\xi}, \quad (10)$$

$$\varpi_{e2} = \left\{ \frac{F_c(k, \varepsilon)}{\mathbf{a}(k)}\Gamma_{01}(t) + \frac{F_a(k, \varepsilon)}{\mathbf{a}(k)}[\Gamma_{02}(t) + \Gamma_{12}(t)] \right\} e^{-ik(\xi-\varepsilon)}, \quad (11)$$

where the functions F_a , F_b , F_c , and \mathbf{a} are given in Appendix A. For the contribution of the vorticity on each foil coming from the vorticity on the other one we use the same simplifying assumption discussed in Ref. [30]. The resulting circulation $\Gamma_{12}(t)$ associated with the contribution of the forewing vorticity distribution on the hindwing vorticity distribution can be written as

$$\Gamma_{12}(t) \simeq \Gamma_{01}f_\Gamma(\varepsilon) - \mathcal{V}_1f_{\Gamma\alpha}(\varepsilon) - \dot{\mathcal{D}}_1f_{\Gamma\delta}(\varepsilon), \quad (12)$$

where the first two terms are similar to those in the case of rigid foils, with α_1 substituted now by $-\mathcal{V}_1$ in the term multiplied by the function $f_{\Gamma\alpha}(\varepsilon)$. The last additional new term is associated with the front foil deflection motion \mathcal{D}_1 , with the new function $f_{\Gamma\delta}(\varepsilon)$ given in Appendix A, together with the functions $f_{\Gamma}(\varepsilon)$ and $f_{\Gamma\alpha}(\varepsilon)$, already given in Ref. [30], for completeness and easy reference.

The different vorticity distributions remain formally the same as those derived in Ref. [30], but using the expressions (8)–(12). Of special relevance for understanding the propulsive enhancement of the back foil owing to its aerodynamic interaction with the front foil (see Sec. V below) is the vorticity distribution on the trailing foil associated with the front-foil wake, which can be written as

$$\varpi_{se12}(x, t) = \frac{1}{\pi} \sqrt{\frac{1-x}{1+x}} \left[\int_{1+\varepsilon}^{\infty} \sqrt{\frac{\xi+1-\varepsilon}{\xi-1-\varepsilon}} \frac{\varpi_{e1}(\xi, t)}{\xi-x} d\xi - \int_1^{-1+\varepsilon} \sqrt{\frac{\xi+1-\varepsilon}{\xi-1-\varepsilon}} \frac{\varpi_{e1}(\xi, t)}{\xi-x} d\xi \right], \quad (13)$$

where ϖ_{e1} is the vorticity distribution (10) along the front-foil wake.

Once the vorticity distributions and their respective circulations are known, the lift, moment, and thrust on each airfoil can be computed by using the vortex impulse formulation [33,48,49], which for the similar case of a tandem of rigid airfoils is detailed in Ref. [30]. The resulting lift coefficient can be written as

$$C_L^{(i)} \equiv \frac{L^{(i)}}{\frac{1}{2}\rho U^2 c} = \mathcal{L}_0(t) + \Gamma_{01}(t)\mathcal{L}_{01} + [\Gamma_{02}(t) + \Gamma_{12}(t)]\mathcal{L}_{02}, \quad (14)$$

where $L^{(i)}$ is the lift force on foil i per unit span and ρ is the fluid density. The only term that changes in relation to the tandem of rigid foils is $\mathcal{L}_0(t)$, which is given in Appendix B for each foil, along with the expressions for \mathcal{L}_{01} and \mathcal{L}_{02} for easy reference.

In the case of the thrust force, being a quadratic expression of the different components of the foils motion, the new deflection term modifies its general form in relation to the rigid foil version. Thus, the thrust coefficient can be written as

$$C_T^{(i)} \equiv \frac{T^{(i)}}{\frac{1}{2}\rho U^2 c} = \mathcal{E}_i C_L^{(i)} - \mathcal{D}_i C_{Td}^{(i)} + C_{T1}^{(i)} + C_{T2}^{(i)} + C_{Te}^{(i)}, \quad (15)$$

where $T^{(i)}$ is the thrust force on foil i per unit span. This expression mainly differs from that of a tandem of rigid foils in the new term $-\mathcal{D}_i C_{Td}^{(i)}$, which is the projection in the flight direction of the normal force and moment of plate i produced by the flexural motion. The different terms for the front ($i = 1$) and trailing ($i = 2$) foils are the following:

$$C_{Td}^{(1)} = \int_1^{\infty} \frac{\varpi_{e1}}{\sqrt{\xi^2-1}} d\xi + \int_{1+\varepsilon}^{\infty} \frac{\varpi_{e2}}{\sqrt{\xi^2-1}} d\xi + \frac{d}{dt} \int_{-1}^1 \left(x^2 - \frac{1}{2} \right) (\varpi_{01} + \varpi_{21}) dx + \left[\frac{1}{2} + (1+\varepsilon)\sqrt{\varepsilon(\varepsilon+2)} - (1+\varepsilon)^2 \right] \varpi_{e2}(1+\varepsilon, t), \quad (16)$$

$$C_{T1}^{(1)} = -\dot{\mathcal{E}}_1 \int_{-1}^1 x(\varpi_{01} + \varpi_{21}) dx - \dot{\mathcal{D}}_1 \int_{-1}^1 \left(x^2 - \frac{1}{2} \right) (\varpi_{01} + \varpi_{21}) dx, \quad (17)$$

$$C_{T2}^{(1)} = \int_1^{\infty} [\dot{\mathcal{J}}_1 + \mathcal{E}_1 - (\dot{\mathcal{E}}_1 + 2\mathcal{D}_1 + \xi\dot{\mathcal{D}}_1)(\sqrt{\xi^2-1} - \xi)] \varpi_{e1} d\xi, \quad (18)$$

$$C_{Te}^{(1)} = - \int_{1+\varepsilon}^{\infty} \left[\frac{\dot{\mathcal{D}}_1}{2} + (\dot{\mathcal{E}}_1 + 2\mathcal{D}_1 + \xi\dot{\mathcal{D}}_1)(\sqrt{\xi^2-1} - \xi) \right] \varpi_{e2} d\xi, \quad (19)$$

$$C_{Td}^{(2)} = \int_{-1+\varepsilon}^{\infty} \frac{\varpi_{e1} + \varpi_{e2}}{\sqrt{(\xi-\varepsilon)^2-1}} d\xi - \int_1^{-1+\varepsilon} \frac{\varpi_{e1}}{\sqrt{(\xi-\varepsilon)^2-1}} d\xi + \frac{d}{dt} \int_{-1+\varepsilon}^{1+\varepsilon} \left[(x-\varepsilon)^2 - \frac{1}{2} \right] (\varpi_{02} + \varpi_{12}) dx$$

$$+ \left[\frac{1}{2} - (1 - \varepsilon)\sqrt{\varepsilon(\varepsilon - 2)} - (1 - \varepsilon)^2 \right] \varpi_{e1}(1, t) + \varpi_{e1}(-1 + \varepsilon, t) - \varpi_{e1}(1 + \varepsilon, t), \quad (20)$$

$$C_{T1}^{(2)} = -\dot{\mathcal{E}}_2 \int_{-1+\varepsilon}^{1+\varepsilon} (x - \varepsilon)(\varpi_{02} + \varpi_{12})dx - \dot{\mathcal{D}}_2 \int_{-1+\varepsilon}^{1+\varepsilon} \left[(x - \varepsilon)^2 - \frac{1}{2} \right] (\varpi_{02} + \varpi_{12})dx, \quad (21)$$

$$C_{T2}^{(2)} = \int_{1+\varepsilon}^{\infty} [\dot{\mathcal{F}}_2 + \mathcal{E}_2 - (\dot{\mathcal{E}}_2 + 2\mathcal{D}_2 + (\xi - \varepsilon)\dot{\mathcal{D}}_2)(\sqrt{(\xi - \varepsilon)^2 - 1} - (\xi - \varepsilon))] \varpi_{e2}d\xi, \quad (22)$$

$$C_{Te}^{(2)} = - \int_{1+\varepsilon}^{\infty} (\dot{\mathcal{E}}_2 + 2\mathcal{D}_2 + (\xi - \varepsilon)\dot{\mathcal{D}}_2)(\sqrt{(\xi - \varepsilon)^2 - 1} - (\xi - \varepsilon)) \varpi_{e1}d\xi \\ + \int_1^{-1+\varepsilon} (\dot{\mathcal{E}}_2 + 2\mathcal{D}_2 + (\xi - \varepsilon)\dot{\mathcal{D}}_2)(\sqrt{(\xi - \varepsilon)^2 - 1} + (\xi - \varepsilon)) \varpi_{e1}d\xi - \frac{\dot{\mathcal{D}}_2}{2} \int_1^{\infty} \varpi_{e1}d\xi. \quad (23)$$

Solving the different integrals, the thrust coefficient can be written as

$$C_T^{(i)} = \mathcal{E}_i C_L^{(i)} + \dot{\mathcal{E}}_i \mathcal{T}_0 + \mathcal{D}_i \mathcal{T}_{\delta 1} + \dot{\mathcal{D}}_i \mathcal{T}_{\delta 2} + \Gamma_{01} \mathcal{T}_{01} + [\Gamma_{02} + \Gamma_{12}] \mathcal{T}_{02}, \quad (24)$$

where all \mathcal{T} functions are different from their rigid foil counterparts and given in Appendix B.

In the case of the moment coefficient, its general form remains the same as that of the tandem of rigid foils, as it happens for the lift coefficient, since both are linear functions of the foil's harmonic motion. If $M^{(i)}$ is the moment that the fluid exerts on the foil i per unit span about the pivot point a_i , the corresponding moment coefficient is given by

$$C_M^{(i)} \equiv \frac{M^{(i)}}{\frac{1}{2}\rho U^2 c^2} = \frac{a_i}{2} C_L^{(i)} + \mathcal{M}_0(t) + \Gamma_{01}(t) \mathcal{M}_{01} + [\Gamma_{02}(t) + \Gamma_{12}(t)] \mathcal{M}_{02}, \quad (25)$$

where only the function $\mathcal{M}_0(t)$ changes when including the flexural motions, and it is given in Appendix B, together with \mathcal{M}_{01} and \mathcal{M}_{02} , already given in Ref. [30], for easy reference.

Finally, for the input power coefficient, a new term associated with the deflection appears in relation to the tandem of rigid foils (already obtained for an isolated foil in Ref. [46]):

$$C_P^{(i)} = -\dot{h}_i C_L^{(i)} - 2\dot{\alpha} C_M^{(i)} - \dot{\delta}_i C_F^{(i)}, \quad (26)$$

where the flexural coefficient $C_F^{(i)}$ is given by

$$C_F^{(1)} = p_1 (4C_{Mp}^{(1)} - p_1 C_L^{(1)}) + \frac{C_{L2}^{(1)}}{2} + \int_{-1}^1 x^2 (\varpi_{01} + \varpi_{21}) dx - \frac{1}{3} \frac{d}{dt} \int_{-1}^1 x^3 (\varpi_{01} + \varpi_{21}) dx \\ + \frac{1}{3} \left[(1 + \varepsilon)^3 - \left((1 + \varepsilon)^2 + \frac{1}{2} \right) \sqrt{\varepsilon(\varepsilon + 2)} \right] \varpi_{e2}(1 + \varepsilon, t) \quad (27)$$

for the front foil, and

$$C_F^{(2)} = p_2 (4C_{Mp}^{(2)} - p_2 C_L^{(2)}) + \frac{C_{L2}^{(2)}}{2} + \frac{1}{2} \int_{-1+\varepsilon}^{1+\varepsilon} \varpi_{e1} d\xi + \int_{-1+\varepsilon}^{1+\varepsilon} (x - \varepsilon)^2 (\varpi_{02} + \varpi_{12}) dx \\ - \frac{1}{3} \frac{d}{dt} \int_{-1+\varepsilon}^{1+\varepsilon} (x - \varepsilon)^3 (\varpi_{02} + \varpi_{12}) dx + \frac{1}{3} [\varpi_{e1}(-1 + \varepsilon, t) + \varpi_{e1}(1 + \varepsilon, t)] \\ + \frac{1}{3} \left[(1 - \varepsilon)^3 + \left((1 - \varepsilon)^2 + \frac{1}{2} \right) \sqrt{\varepsilon(\varepsilon - 2)} \right] \varpi_{e1}(1, t) \quad (28)$$

for the trailing foil. Solving these expressions, they can be written as

$$C_F^{(i)} = p_i [4C_{Mp}^{(i)} - p_i C_L^{(i)}] + \mathcal{F}_0(t) + \Gamma_{01}(t) \mathcal{F}_{01} + [\Gamma_{02}(t) + \Gamma_{12}(t)] \mathcal{F}_{02}, \quad (29)$$

where $C_{Mp}^{(i)}$ is the moment coefficient (25) replacing $a_i/2$ by $p_i/2$ in its first term, and the different functions and coefficients $\mathcal{F}_0(t)$, \mathcal{F}_{01} , and \mathcal{F}_{02} are summarized in Appendix B.

B. Time-averaged coefficients

For practical purposes, one is mostly interested in the time-averaged coefficients, defined as

$$\bar{C}^{(i)} = \frac{k}{2\pi} \int_t^{t+2\pi/k} C^{(i)}(t) dt, \quad (30)$$

where $C^{(i)}$ is any of the above coefficients for the foil i . Thus, the time-averaged thrust and input power coefficients can be decomposed into two terms,

$$\bar{C}_T^{(i)} = \bar{C}_{Tr}^{(i)} + \bar{C}_{Td}^{(i)}, \quad \bar{C}_P^{(i)} = \bar{C}_{Pr}^{(i)} + \bar{C}_{Pd}^{(i)}, \quad (31)$$

where $\bar{C}_{Tr}^{(i)}$ and $\bar{C}_{Pr}^{(i)}$ are the mean thrust and input power, respectively, of each foil as if they were rigid foils, and $\bar{C}_{Td}^{(i)}$ and $\bar{C}_{Pd}^{(i)}$ are the contributions from the deflection motion. The rigid-foil contributions, obtained in Ref. [30], can be formally written as

$$\bar{C}_{Tr}^{(i)} = (kh_{0i})^2 \{t_h(k, \varepsilon, \varphi, \Theta_h) + t_c(k, \varepsilon, \varphi, \phi_i, \phi_j, a_i, a_j, \Theta_h, \Theta_a)\theta_i + t_p(k, \varepsilon, \varphi, a_i, a_j, \Theta_a)\theta_i^2\}, \quad (32)$$

$$\bar{C}_{Pr}^{(i)} = (kh_{0i})^2 \{p_h(k, \varepsilon, \varphi, \Theta_h) + p_c(k, \varepsilon, \varphi, \phi_i, \phi_j, a_i, a_j, \Theta_h, \Theta_a)\theta_i + p_p(k, \varepsilon, \varphi, a_i, a_j, \Theta_a)\theta_i^2\}, \quad (33)$$

while the new contributions from the flexural motion can be written in a similar fashion as

$$\begin{aligned} \bar{C}_{Td}^{(i)} = & (kh_{0i})^2 \{[t_{hd}(k, \varepsilon, \varphi, p_i, p_j, \psi_i, \psi_j, \Theta_h, \Theta_d) \\ & + t_{pd}(k, \varepsilon, \varphi, a_i, a_j, p_i, p_j, \phi_i, \phi_j, \psi_i, \psi_j, \Theta_a, \Theta_d)\theta_i]\theta_{di} \\ & + t_d(k, \varepsilon, \varphi, p_i, p_j, \psi_i, \psi_j, \Theta_d)\theta_{di}^2\}, \end{aligned} \quad (34)$$

$$\begin{aligned} \bar{C}_{Pd}^{(i)} = & (kh_{0i})^2 \{[p_{hd}(k, \varepsilon, \varphi, p_i, p_j, \psi_i, \psi_j, \Theta_h, \Theta_d) \\ & + p_{pd}(k, \varepsilon, \varphi, a_i, a_j, p_i, p_j, \phi_i, \phi_j, \psi_i, \psi_j, \Theta_a, \Theta_d)\theta_i]\theta_{di} \\ & + p_d(k, \varepsilon, \varphi, p_i, p_j, \psi_i, \psi_j, \Theta_d)\theta_{di}^2\}, \end{aligned} \quad (35)$$

where

$$\theta_i = \frac{a_{0i}}{kh_{0i}}, \quad \theta_{di} = \frac{d_{mi}}{kh_{0i}}, \quad (36)$$

are the feathering parameters of each foil and the equivalent ones for the flexural amplitudes, and

$$\Theta_h = \frac{h_{0j}}{h_{0i}}, \quad \Theta_a = \frac{a_{0j}}{a_{0i}}, \quad \Theta_d = \frac{d_{mj}}{d_{mi}}, \quad (37)$$

are amplitude ratios. All the new functions t_{hd} , t_d , p_{hd} , and p_d for each airfoil are given in the Supplemental Material [47], together with the rigid-foil ones t_h , t_c , t_p , p_h , p_c , and p_p for easy reference.

Finally, the propulsive efficiency of each foil is conveniently written in terms of these functions and the feathering parameters:

$$\eta_i = \frac{\bar{C}_T^{(i)}}{\bar{C}_P^{(i)}} = \frac{t_h + t_{ph}\theta_i + t_p\theta_i^2 + (t_{hd} + t_{pd}\theta_i)\theta_{di} + t_d\theta_{di}^2}{p_h + p_{ph}\theta_i + p_p\theta_i^2 + (p_{hd} + p_{pd}\theta_i)\theta_{di} + p_d\theta_{di}^2}. \quad (38)$$

The global time-averaged thrust and efficiency of the tandem are defined as

$$\bar{C}_T = \bar{C}_T^{(1)} + \bar{C}_T^{(2)}, \quad \eta = \frac{\bar{C}_T^{(1)} + \bar{C}_T^{(2)}}{\bar{C}_P^{(1)} + \bar{C}_P^{(2)}}. \quad (39)$$

IV. VALIDATION

The thrust force coefficient and the corresponding propulsive efficiency, resulting from the vortex impulse theory in the linear potential flow limit which is used here, valid for sufficiently high Reynolds numbers and small amplitudes, has been widely tested with experimental and numerical data from different sources for pitching and heaving rigid foils. These tests have been reported in Refs. [33,50–53] for isolated rigid foils, and in Ref. [30] for a tandem configuration of rigid heaving foils, where experimental results by Ramanarivo *et al.* [23] and by Newbolt *et al.* [26] were favorably compared with the results from the present linear potential theory (see also immediately below). Another validation of the theory for two pitching rigid foils in tandem configuration is provided in the present work by comparing with numerical simulations by Boschitsch *et al.* [21] (see Sec. VI B and Fig. 7 below).

For the case of a single foil with prescribed quadratic flexural deflection like the one considered in the present work, the results have been validated against numerical and experimental data in Ref. [46].

For a tandem flapping flexible foils, the available numerical or experimental data for validation is scarce, especially for high-enough Reynolds numbers and small amplitude, with the additional difficulty that most of the published works do not provide information about the flexural deflection amplitudes and phase, d_{mi} and ψ_i , which are needed to evaluate the force expressions derived in this work. However, like in the rigid-foil case, available results for the equilibrium separation distances between two self-propelled plates in tandem arrangement can be used as an alternative. Thus, in Ref. [30] we showed that the equilibrium separations between two self-propelled heaving rigid plates in tandem arrangement found experimentally by Ramanarivo *et al.* [23] and by Newbolt *et al.* [26] correspond to configurations with maximum amplification of the tandem propulsive efficiency computed from the linear potential theory.

The recent work by Ryu *et al.* [45], with numerical simulations for two self-propelled heaving flexible plates in a tandem arrangement, reports such kind of results in the separation-phase plane ($\tilde{d}/c-\varphi$ plane, where the *tilde* over d means dimensional quantity). Figure 2 shows that, similarly to the results reported in Ref. [30] for rigid foils, the bands of maximum propulsive efficiency of the tandem obtained with the present theory roughly correspond to equilibrium separation distances between the self-propelled plates obtained numerically by Ryu *et al.* [45]. The results given by these authors are for flexible plates with the conditions given in the caption of Fig. 2 but, since no data can be extracted for d_m or ψ from their reported results, they are compared in Fig. 2 with the efficiency amplification obtained from the present theory for both a tandem of rigid foils and a tandem of flexible foils with the same kinematics of the reported numerical results and selected values of the flexural deflection amplitude and phase. The normalized efficiencies plotted in this figure are

$$\hat{\eta} = \frac{\eta_r}{\eta_s} \quad \text{and} \quad \tilde{\eta} = \frac{\eta}{\eta_r}, \quad (40)$$

for rigid foils and flexible foils, respectively, where η is the total efficiency defined in Eq. (39), the subscript s stands for a single airfoil undergoing the same motion, and the subscript r , as in Sec. III B above, means rigid foils, for which we use the same expression (39) but setting to zero the flexural deflection amplitude d_m . Although the contour values inside the bands of efficiency amplification and reduction are obviously different in each case, the slope and location of the banded patterns are practically the same and agree quite well with the numerical results by Ryu *et al.* [45]. It should be noted that, although the amplitude $h_0 = 0.4$ does not seem sufficiently small for a linear theory, the present theory for pure heave of a single airfoil works remarkably well even for not too small

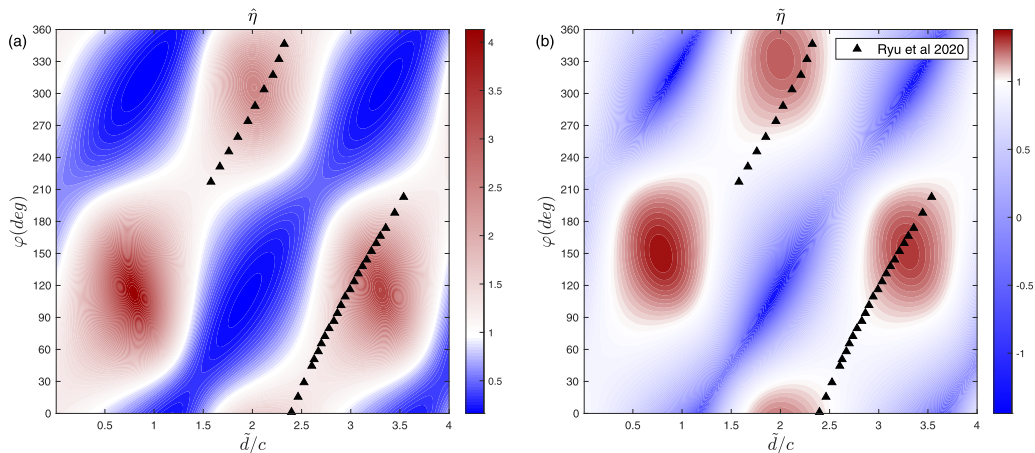


FIG. 2. Contours of the normalized propulsive efficiency in the \tilde{d}/c - φ plane for tandem heaving foils with $k = 1.25$ and $p = -1$. (a) $\tilde{\eta}$ for a pair of rigid foils. (b) $\tilde{\eta}$ for a pair of flexible foils with $d_m/h_0 = 1/4$ and $\psi = 90^\circ$. The symbols correspond to equilibrium gap distances obtained by Ryu *et al.* [45] in their numerical simulations for two self-propelled flexible plates in tandem for the same values of k and p , and $h_0 = 0.4$ [i.e., their tandem flapping (TF) modes in Fig. 2(d) of Ref. [45]; note that their \bar{G}_x is our $\tilde{d}/c + 1$, while their $\Delta\phi$ is our φ].

amplitudes, as shown in Ref. [33] comparing theoretical results for the thrust coefficient and the efficiency with experimental data by Heathcote and Gursul [35] for $h_0 = 0.35$.

As already mentioned, similar patterns for the maxima in the efficiency enhancement, but now in the separation-frequency plane \tilde{d}/c - k , were found in Ref. [30] for a tandem arrangement of heaving rigid foils in phase. As shown experimentally by Ramanarivo *et al.* [23], these aerodynamic amplification modes correspond to equilibrium separation distances which are integer multiples of the front-foil wake wavelength. This was characterized by these authors by defining the so-called schooling number, or ratio between the separation \tilde{d} and the wavelength $\lambda = \pi c/k$ of the wake,

$$S = \frac{\tilde{d}}{\lambda} = \frac{dk}{2\pi}. \quad (41)$$

These patterns are also found here for flexible flapping foils in tandem (see Sec. VI below), with different propulsive amplifications depending on the flexural deflection amplitude and phase. But before presenting these results, we explore in the following section the physics behind such regular patterns of the maxima in the efficiency enhancement, according to the present theory, and how this amplification is affected by the flexural motion.

V. ANALYSIS OF THE IMPACT OF THE UPSTREAM WAKE ON THE BACK-FOIL THRUST

The main contribution to the amplification (or reduction) in the propulsion capabilities of flapping foils in tandem configuration, in relation to an isolated flapping foil, obviously comes from the interaction of the front-foil wake with the back foil, which may enhance (or reduce) the thrust generated by the trailing foil in relation to a single foil undergoing the same motion, and therefore increase (or reduce) the propulsive efficiency of the tandem system. In the present linear potential theory, where no leading- or trailing-edge vortices are intermittently shed by the flapping foils, but vorticity is continuously shed in concentrated free (wake) vortex sheets, in addition to the vorticity inside the thin bound vortex sheets on the flapping foils, this contribution is characterized by Eq. (13), or contribution to the vorticity distribution along the back foil, ϖ_{s2} , due to the vorticity distribution ϖ_{e1} in the upstream wake.

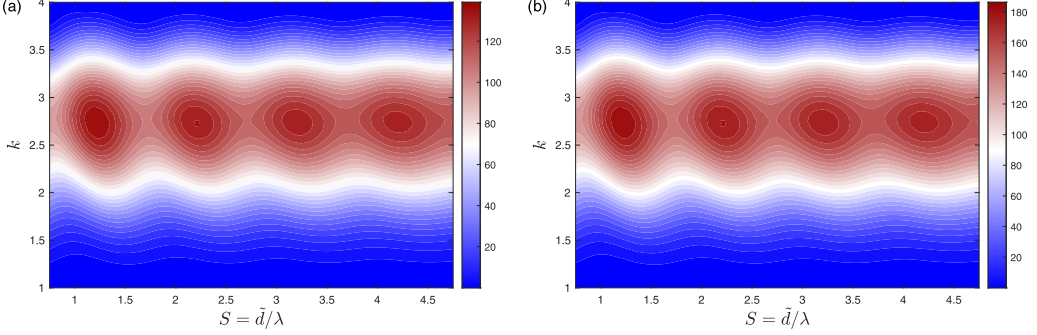


FIG. 3. Contour values of \mathcal{M}/h_0^2 in the schooling number-frequency plane for purely heaving (a) rigid and (b) flexible foils with $d_m/h_0 = 1/4$, $\psi = \varphi = 0$, and $p = -1$.

In particular, it is well known that the intensity of the bound vorticity distribution ϖ_s on a plate at the leading edge is related, within the linear potential theory, to the suction force at the leading edge [54]: ϖ_s is singular at the leading edge, but generates a finite suction force. This was used, for example, by Garrick [55] to quantify the suction component of the thrust force generated by a pitching and heaving rigid plate within the linear potential theory. This suction thrust force is given by $T_S = \pi \rho K^2$, where $K = \lim_{x \rightarrow -c/2} \sqrt{x + c/2} \varpi_s(x, t)/2$, for an airfoil with leading edge at $x = -c/2$. Thus, taking into account the above argument and using the present dimensionless variables, the main contribution to the thrust force amplification in the back foil in relation to an isolated foil can be obtained from Eq. (13) when the singularity at the leading edge $x = -1 + \varepsilon$ is removed; i.e., from the quantity

$$m(x, t) := \int_{1+\varepsilon}^{\infty} \sqrt{\frac{\xi + 1 - \varepsilon}{\xi - 1 - \varepsilon}} \frac{\varpi_{e1}(\xi, t)}{\xi - x} d\xi - \int_1^{-1+\varepsilon} \sqrt{\frac{\xi + 1 - \varepsilon}{\xi - 1 - \varepsilon}} \frac{\varpi_{e1}(\xi, t)}{\xi - x} d\xi, \quad (42)$$

which, after substituting the upstream wake vorticity ϖ_{e1} from Eq. (10), results in

$$m(x, t) = \left[\frac{F_a(k, \varepsilon)}{\mathbf{a}(k)} \Gamma_{01}(t) + \frac{F_b(k, \varepsilon)}{\mathbf{a}(k)} (\Gamma_{02}(t) + \Gamma_{12}(t)) \right] \times \left[\int_{1+\varepsilon}^{\infty} \sqrt{\frac{\xi + 1 - \varepsilon}{\xi - 1 - \varepsilon}} \frac{e^{-ik\xi}}{\xi - x} d\xi - \int_1^{-1+\varepsilon} \sqrt{\frac{\xi + 1 - \varepsilon}{\xi - 1 - \varepsilon}} \frac{e^{-ik\xi}}{\xi - x} d\xi \right]. \quad (43)$$

We are interested in the time-averaged value of the square of the real part of this quantity at the leading edge of the back foil, which as argued above characterizes (is proportional to) the main contribution to the nondimensional amplification in the suction thrust of the trailing foil due to the upstream wake:

$$\mathcal{M} := \frac{k}{2\pi} \int_t^{t+2\pi/k} \text{Re}[m(x = -1 + \varepsilon, t)] \text{Re}[m(x = -1 + \varepsilon, t)] dt. \quad (44)$$

The maxima in \mathcal{M} as the geometrical and kinematic parameters are varied and will provide relevant information about the optimal configurations of the tandem in terms of thrust and, most likely, in terms of propulsive efficiency, since the main propulsive advantage of the tandem configuration is the amplification in the thrust force of the trailing foil.

For purely heaving foils with the same amplitude h_0 , \mathcal{M}/h_0^2 depends only on k , d , and φ for rigid foils and additionally on d_m/h_0 , ψ , and p for flexible foils. This quantity is plotted in Fig. 3 as a function of the schooling number (41) and the reduced frequency for rigid foils in phase ($\varphi = 0$), and for flexible foils with $p = -1$ (deflection axis at the leading edge), $d_m/h_0 = 1/4$ and $\psi = 0$.

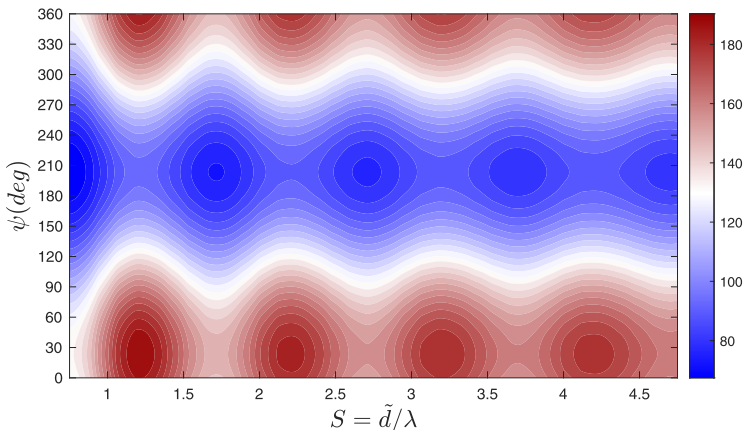


FIG. 4. Contour values of \mathcal{M}/h_0^2 in the schooling number-phase shift plane for heaving plates with flexural deflection amplitude $d_m/h_0 = 1/4$. $\varphi = 0$, $p = -1$, and $k = 2.75$.

It is noticeable that the thrust amplification pattern is the same in both cases, with a frequency band containing peaks at selected values of the schooling number which are slightly larger than the successive natural numbers, in good agreement with the experimental results by Ramanarivo *et al.* [23]. (There exist similar bands at higher frequencies, but only the lowest-frequency one is shown in Fig. 3.) On the other hand, the thrust amplification in the foil with flexural deflection is significantly larger than that of a rigid foil for the selected values of the parameters. In fact, $p = -1$ is usually the best deflexion axis location in terms of propulsion performance of a foil with quadratic flexural deflection [30], and the thrust increases quadratically with d_m in the present linear theory, so that most the relevant parameter to quantify the effect of the flexural motion on the thrust enhancement for given φ is the phase shift ψ between the heaving and flexural motions. Figure 4 shows the effect of ψ on \mathcal{M}/h_0^2 for the optimal frequency in Fig. 3 ($k \simeq 2.75$). It is observed that the optimal phase shift for thrust enhancement of the trailing foil due to its interaction with the upstream wake is about 25° , close to the case plotted in Fig. 3.

It must be remarked that this analysis considers only the (arguably) most relevant contribution to the suction force at the leading edge of the trailing foil, not all contributions to the total thrust force. But it serves to illustrate the physical origin of the thrust (and efficiency) enhancement in a tandem configuration in comparison with an isolated foil, and how it can be further augmented by the foil's flexural deflection.

VI. RESULTS

Owing to the large number of geometric and kinematic parameters, only the cases of purely heaving or pitching motions pivoting about the leading edges, combined with chordwise deflection, will be considered here with some detail.

A. Purely heaving motion with chordwise deflection

In this case, the time-averaged coefficients reduce to

$$\overline{C}_{Td}^{(i)} = (kh_{0i})^2 \{t_{hd}(k, \varepsilon, \varphi, p_i, p_j, \psi_i, \psi_j, \Theta_h, \Theta_d)\theta_{di} + t_d(k, \varepsilon, \varphi, p_i, p_j, \psi_i, \psi_j, \Theta_d)\theta_{di}^2\}, \quad (45)$$

$$\overline{C}_{Pd}^{(i)} = (kh_{0i})^2 \{p_{hd}(k, \varepsilon, \varphi, p_i, p_j, \psi_i, \psi_j, \Theta_h, \Theta_d)\theta_{di} + p_d(k, \varepsilon, \varphi, p_i, p_j, \psi_i, \psi_j, \Theta_d)\theta_{di}^2\}. \quad (46)$$

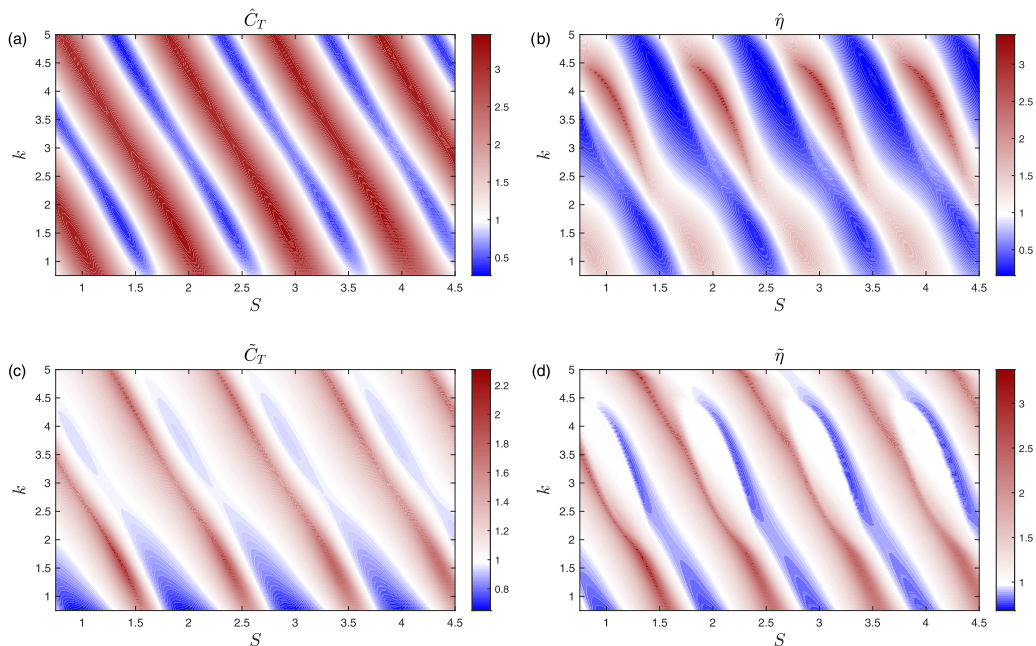


FIG. 5. Contours of normalized thrust (left panels) and normalized propulsive efficiency (right panels) of the tandem in the \tilde{d}/c - k plane for pure heave with $\varphi = 0$ and $p = -1$. Panels (a) and (b) are for a tandem of rigid foils, with quantities normalized by those of an otherwise identical single foil. Panels (c) and (d) are for a tandem of flexible foils with chordwise deflection when $d_m/h_0 = 1/4$ and $\psi = 270^\circ$, now normalized by the corresponding values for the tandem of rigid foils.

To simplify further, we shall consider the same heaving and deflection amplitudes for both plates ($\Theta_h = \Theta_d = 1$), with the same phase shifts ($\psi_1 = \psi_2 = \psi$) and pivoting about their leading edges ($p_1 = p_2 = p = -1$).

First we compare in Fig. 5 the patterns of thrust and efficiency enhancement (or reduction) in the schooling number-frequency plane for the rigid-foil case with the present results when chordwise deflection is added. The normalized efficiencies are defined in Eq. (40), while the normalized time-averaged thrust coefficients are similarly defined as

$$\hat{C}_T = \frac{\bar{C}_{Tr}}{\bar{C}_{Ts}} \quad \text{and} \quad \tilde{C}_T = \frac{\bar{C}_T}{\bar{C}_{Tr}}, \quad (47)$$

for rigid foils and flexible foils, respectively, where \bar{C}_T is the total thrust coefficient defined in Eq. (39), the subscript s stands for a single foil undergoing the same motion, and the subscript r means rigid foils, for which we use the same expression (39) but setting to zero the flexural deflection amplitude d_m . All the normalized quantities are independent of the amplitude of the oscillations, in this case of the heave amplitude h_0 . It must be noted that, although the magnitude of the amplifications in Fig. 5 seems unrealistic in some cases, these amplifications are in relation to the isolated rigid foil in Figs. 5(a) and 5(c), or to the tandem of rigid foils in Figs. 5(b) and 5(d), for the *same* values of k and S , which obviously do not always coincide with their respective maxima.

For comparison's sake, Figs. 5(a) and 5(b) reproduce results from Ref. [30] for a tandem of rigid foils in phase ($\varphi = 0$), but now in the S - k plane, with S defined in Eq. (41), instead of the \tilde{d}/c - k plane. As shown in Ref. [30], the maxima in the efficiency magnification shown in Fig. 5(b) approximately follow the multiple arrangements that self-propelled foils undergoing a

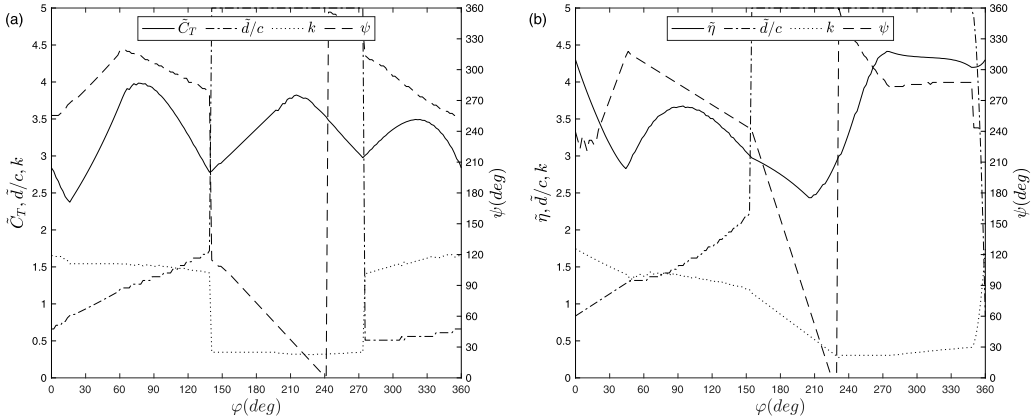


FIG. 6. Maxima in (a) \bar{C}_T and (b) $\bar{\eta}$ within the first amplification modes (with lower frequencies) plotted in Figs. 5(c) and 2(d), respectively, as a function of the phase shift φ and the corresponding optimal values of k , \bar{d}/c , and ψ .

heaving motion at high Reynolds numbers spontaneously assume due to flow interactions, roughly corresponding to integer values of the schooling number [23].

Figures 5(c) and 5(d) show the corresponding normalized quantities for a tandem arrangement of heaving foils with flexural deflection amplitude $d_m/h_0 = 1/4$ and phase shift $\psi = 270^\circ$. It is observed that the amplification pattern remains, now in relation to the tandem rigid foils, but with a slight shift in the S - k plane that partially overlaps the adjacent regions of reduction in the propulsive performance of the tandem rigid foils. For given φ , this shift in the amplification pattern depends on the flexural deflection phase ψ . For the case $\psi = 270^\circ$ plotted in Figs. 5(c) and 5(d), the net effect is that a quadratic deflection may augment further the thrust and the propulsive efficiency of the tandem arrangement in several banded regions of the S - k plane. Particularly relevant is the first amplification mode (lower S), especially at the lowest frequencies, which are the most interesting conditions from a physical point of view, and for that reason is explored with more detail next.

Figure 6 plots the maximum values of the thrust and efficiency corresponding to the first amplification mode with the lowest frequencies shown in Figs. 5(c) and 5(d) as the phase shift φ is varied from the value $\varphi = 0$ used in Fig. 5, maintaining the flexural deflection amplitude $d_m/h_0 = 1/4$ and varying also the deflection phase shift ψ . This figure also contains the corresponding optimal values of k , \bar{d}/c , and ψ for both thrust and efficiency enhancement by flexibility. Note that the deflection amplitude is not varied because the thrust coefficient goes as d_m^2 and the efficiency is almost independent of d_m in the present linear theory. The maximum thrust enhancement by flexibility is obtained for a heave phase shift $\varphi \approx 75^\circ$, corresponding to $k \approx 1.5$, $\psi \approx 300^\circ$, and $\bar{d}/c \approx 1.25$. For a similar value of φ there is a local peak of efficiency enhancement which, although it is not the absolute maximum in Fig. 6(b), it is the most interesting one in view of the corresponding optimal values of the parameters. It is obtained with practically the same values of φ , k , and ψ of the maximum thrust, but for a slightly larger separation, about 1.5 chord lengths. The other local maxima of thrust and efficiency enhancement are less interesting physically because they are obtained for either too large or too low separations between the foils, for which the present inviscid theory is less accurate. Thus, although there are other local maxima in the efficiency or in the thrust force amplifications, this one appears within the range of physically relevant values of the parameters where the present theory is more accurate and it is robust in the sense that both thrust and efficiency enhancement reach local maxima at these optimal conditions.

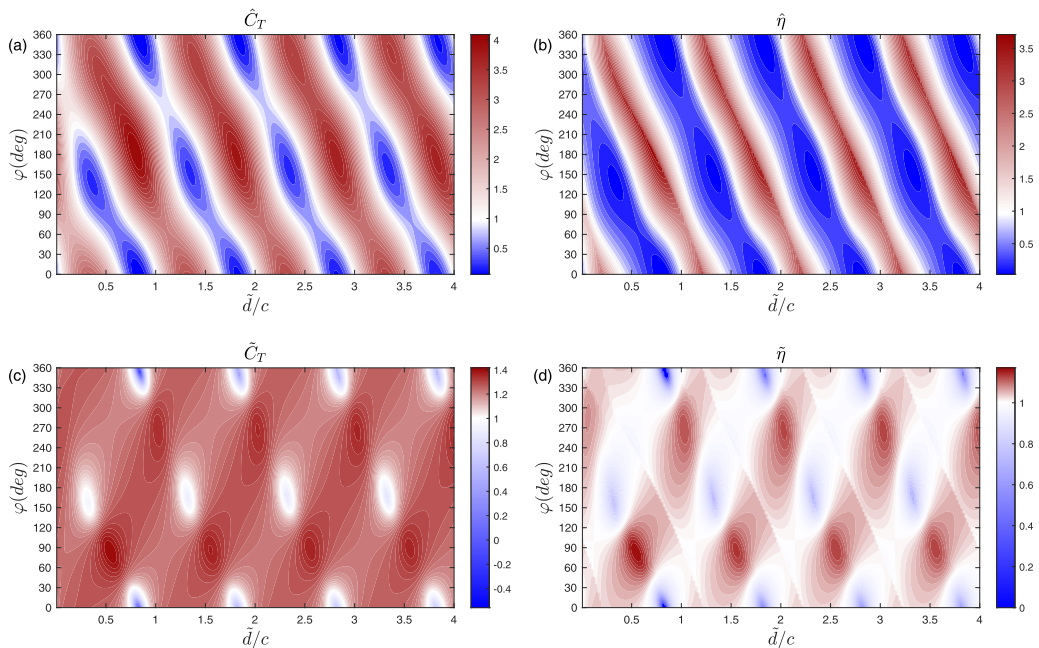


FIG. 7. Contours of the tandem normalized thrust (left panels) and the tandem normalized propulsive efficiency (right panels) in the \tilde{d}/c - φ plane for purely pitching motions with $k = \pi$ and $a = p = -1$. Panels (a) and (b) are for a tandem of rigid foils, with quantities normalized by those of an otherwise identical single foil, while panels (c) and (d) are for a tandem of flexible foils with trailing-edge deflection amplitude $d_m/a_0 = 1/4$ and $\psi = 180^\circ$, now normalized by the corresponding values for the tandem of rigid foils.

B. Purely pitching motion with chordwise deflection

Banded patterns of enhancement (or reduction) of the tandem propulsive performance in the S - k plane (or the \tilde{d}/c - k plane) are also observed for pitching foils. However, we shall present now the results in the spacing-phase shift plane following Boschitsch *et al.* [21], who used it to discuss their experimental results for a similar configuration of pitching rigid plates. This \tilde{d}/c - φ plane was already used in Fig. 2 for two heaving foils, showing angled bands of propulsive enhancement. In fact, Boschitsch *et al.* [21] were the first to observe these angled band patterns experimentally for the thrust amplification of the trailing foil in an in-line configuration of rigid foils pitching about their leading edges.

Figure 7 shows the contours in the \tilde{d}/c - φ plane of the normalized thrust coefficient and propulsive efficiency of a tandem arrangement of both rigid and flexible foils pitching about their leading edges ($a_1 = a_2 = a = -1$) at the same reduced frequency $k = \pi$ of the results reported in Fig. 8 of Ref. [21]. Note that now, in the absence of heaving motion, φ is the phase lag between the pitching motions. The coefficients are normalized according to Eqs. (40) and (47), thus independent of the pitch amplitude a_0 . Boschitsch *et al.* [21] plotted in their Fig. 8 the same normalized values but for the downstream foil. However, since the trailing foil is by far the main contributor to the tandem thrust and efficiency enhancement, the banded patterns in Figs. 7(a) and 7(b) for rigid foils practically coincide with those reported in Fig. 8 of Boschitsch *et al.* [21], but obviously with different contour values since we are representing different quantities.

Similarly to the case of purely heaving motions, for pitching foils with quadratic chordwise deflection, we consider only configurations with the same pitching and deflection amplitudes for both plates ($\Theta_a = \Theta_d = 1$), with the same deflection phase shifts ($\psi_1 = \psi_2 = \psi$) and pivoting about their leading edges ($a_1 = a_2 = a = p_1 = p_2 = p = -1$). Figures 7(c) and 7(d) show the

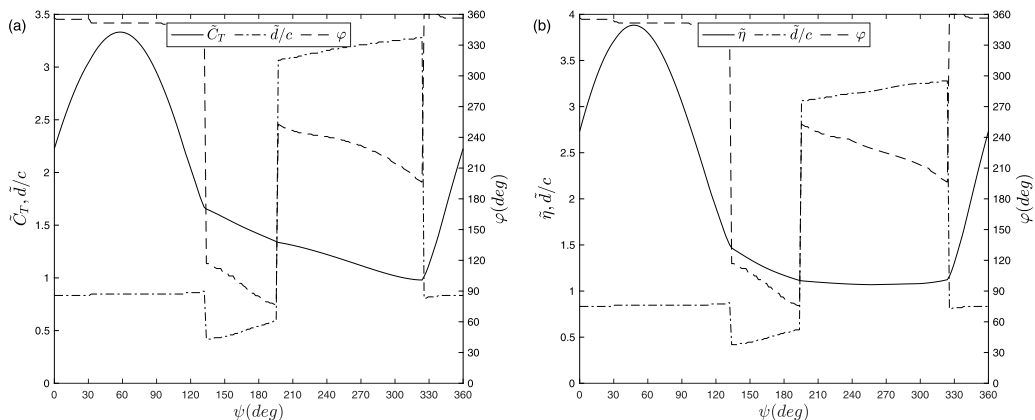


FIG. 8. Maxima in (a) \tilde{C}_T and (b) $\tilde{\eta}$ in the first amplification modes plotted in Figs. 7(c) and 7(d), respectively, as a function of the deflection phase shift ψ and the corresponding optimal values of φ and \tilde{d}/c . $k = \pi$.

effect of a quadratic flexural deflection on the rigid-foil case plotted in Figs. 7(a) and 7(b) when the deflection amplitude is $d_m/a_0 = 1/4$ and its phase shift $\psi = 180^\circ$. The banded patterns for thrust and efficiency basically remain, but with spots of thrust and efficiency enhancement by the quadratic deflection in relation to their rigid foil counterparts.

Figure 8 shows the maxima in the thrust and efficiency enhancement corresponding to the first amplification mode shown in Figs. 7(c) and 7(d) as the deflection phase shift ψ is varied [note that $\psi = 180^\circ$ in Figs. 7(c) and 7(d)], maintaining the flexural deflection amplitude at $d_m/a_0 = 1/4$ and the reduced frequency at $k = \pi$. This figure also contains the corresponding optimal values of \tilde{d}/c and φ for both thrust and efficiency enhancement by flexural deformation. The deflection amplitude is not varied because the thrust coefficient increases quadratically with d_m/a_0 and the efficiency is almost independent of d_m/a_0 in the present linear theory. The maximum thrust and efficiency enhancement by flexural deflection are both obtained at roughly the same values of the parameters, namely $\psi \approx 60^\circ$, $\tilde{d}/c \approx 0.8$, and $\varphi \approx 350^\circ$. This optimal separation and the selected frequency are well within the range of validity of the present theory and this maximum is robust in the sense that at these optimal conditions both thrust and efficiency enhancement reach local maximum values.

VII. CONCLUSIONS

We have analyzed the effect of chordwise flexural deflection on the propulsive performance of a tandem arrangement of two-dimensional flapping foils in the linearized inviscid limit. General expressions for the vorticity distributions, the thrust, moment, power input, and propulsive efficiency are given analytically in terms of the huge number of geometric and kinematic parameters characterizing the complex aerodynamic problem. This is the main advantage of the present approach: although limited to small amplitudes of the flapping and deflection motions and to high Reynolds number flows, the effect on the propulsive performance of all these parameters is readily available, while in numerical and experimental studies only the effect of a very reduced number of parameters can be taken into account simultaneously. In addition, we use the analytical expressions for the vorticity distributions to analyze the effect of the front-foil wake on the thrust of the trailing foil, thus extracting relevant qualitative information about the optimal configurations for thrust and efficiency enhancement, both for a tandem of rigid foils and for the case with the additional flexural deflection.

From these general expressions, we have presented results for two particular configurations consisting of purely heaving and purely pitching motions of the foils about their leading edges. These configurations have been selected because there exists a good agreement with available

experimental and numerical data for the case of rigid foils, some of these validations made in a previous work for tandem rigid foils [46], and new comparisons presented here. We have analyzed with some detail how a small-amplitude chordwise deflection improves the propulsive performance of the tandem flapping foils. For heaving foils we find that thrust enhancement by flexibility is maximized for a phase shift between the two heaving motions of about 75° , for a separation distance about 1.25 chord lengths, a reduced frequency around 1.5, and a deflection phase shift of about 300° . Maximum propulsive efficiency enhancement is obtained for basically the same values of these parameters, but for a slightly larger spacing between the foils. For pitching foil about their leading edges we have selected a particular value of the reduced frequency to compare with a previous experimental work for rigid foils [21] and find that both the maximum thrust and the maximum efficiency enhancement by flexural deflection is obtained for almost in-phase pitching foils, separated a little less than one chord length and with a deflection phase shift of about 60° . All these results, both the general analytical expressions and the findings for the particular flapping configurations, may be of interest as a first guide in the design of small aerial or aquatic vehicles using tandem propulsors.

ACKNOWLEDGMENT

This research was supported by the Ministerio de Economía y Competitividad of Spain Grant No. DPI2016-76151-C2-1-R.

APPENDIX A: SOME INTEGRALS AND FUNCTIONS

The integrals and functions used in deriving the results of the paper are summarized here:

$$\mathcal{A}_1(k, \varepsilon) \equiv \int_{1-\varepsilon}^{-1} \frac{e^{-ik(\xi+\varepsilon)}}{\sqrt{\xi^2-1}} d\xi, \quad \mathcal{A}_2(k, \varepsilon) \equiv \int_{1+\varepsilon}^{\infty} \frac{e^{-ik(\xi-\varepsilon)}}{\sqrt{\xi^2-1}} d\xi, \quad (\text{A1})$$

$$\mathcal{Q}_1(k, \varepsilon) \equiv \int_{1-\varepsilon}^{-1} e^{-ik(\xi+\varepsilon)} \sqrt{\xi^2-1} d\xi, \quad \mathcal{Q}_2(k, \varepsilon) \equiv \int_{1+\varepsilon}^{\infty} e^{-ik(\xi-\varepsilon)} \sqrt{\xi^2-1} d\xi, \quad (\text{A2})$$

$$\mathcal{Q}(k, \varepsilon) \equiv iH_1^{(2)}(k) + \frac{4i}{\pi k} [k \cos(k) - \sin(k)] + \frac{2}{\pi} \frac{e^{ik(\varepsilon-1)}}{k} [1 + ik(1-\varepsilon)], \quad (\text{A3})$$

$$\mathbf{a}(k) \equiv \frac{\pi}{2} [iH_0^{(2)}(k) + H_1^{(2)}(k)], \quad (\text{A4})$$

$$\mathbf{b}(k, \varepsilon) \equiv \frac{i}{k} e^{-ik} + \left(1 + i \frac{d}{dk}\right) \mathcal{A}_2(k, \varepsilon), \quad (\text{A5})$$

$$\mathbf{c}(k, \varepsilon) \equiv \frac{i}{k} e^{-ik} + \left(1 + i \frac{d}{dk}\right) \mathcal{A}_1(k, \varepsilon) - \mathbf{a}(k) e^{-ik\varepsilon}, \quad (\text{A6})$$

$$F_a(k, \varepsilon) \equiv \frac{\mathbf{a}(k)}{\mathbf{a}(k) - \frac{\mathbf{b}(k, \varepsilon)}{\mathbf{a}(k)} \mathbf{c}(k, \varepsilon)}, \quad F_b(k, \varepsilon) \equiv \frac{\mathbf{b}(k, \varepsilon)}{\mathbf{a}(k) - \frac{\mathbf{b}(k, \varepsilon)}{\mathbf{a}(k)} \mathbf{c}(k, \varepsilon)}, \quad (\text{A7})$$

$$F_c(k, \varepsilon) \equiv \frac{\mathbf{c}(k, \varepsilon)}{\mathbf{a}(k) - \frac{\mathbf{b}(k, \varepsilon)}{\mathbf{a}(k)} \mathbf{c}(k, \varepsilon)}, \quad (\text{A8})$$

$$\mathcal{C}_a \equiv 1 - \frac{iH_0^{(2)}(k)F_a(k, \varepsilon)}{iH_0^{(2)}(k) + H_1^{(2)}(k)}, \quad \mathcal{C}_b \equiv -\frac{iH_0^{(2)}(k)F_b(k, \varepsilon)}{iH_0^{(2)}(k) + H_1^{(2)}(k)},$$

$$\mathcal{C}_c \equiv -\frac{iH_0^{(2)}(k)F_c(k, \varepsilon)}{iH_0^{(2)}(k) + H_1^{(2)}(k)}, \quad (\text{A9})$$

$$\mathcal{C}(k) \equiv \frac{H_1^{(2)}(k)}{iH_0^{(2)}(k) + H_1^{(2)}(k)}, \quad \mathcal{C}_1(k) \equiv \frac{\frac{1}{k} e^{-ik}}{iH_0^{(2)}(k) + H_1^{(2)}(k)}, \quad (\text{A10})$$

$$C_{1e}(k, \varepsilon) \equiv \frac{\frac{1}{k}e^{-ik\varepsilon}}{iH_0^{(2)}(k) + H_1^{(2)}(k)}, \quad (\text{A11})$$

$$\mathcal{B}_1(k, \varepsilon) \equiv \frac{\mathcal{Q}_2(k, \varepsilon)}{\mathbf{a}(k)} + \frac{2}{\pi} \left(\frac{1+ik}{k} + i\varepsilon \right) C_1(k), \quad \mathcal{B}_2(k, \varepsilon) \equiv \mathcal{Q}(k, \varepsilon)C_{1e}(k, \varepsilon) - \frac{\mathcal{Q}_1(k, \varepsilon)}{\mathbf{a}(k)}, \quad (\text{A12})$$

where $H_n^{(2)}(z) = J_n(z) - iY_n(z)$, $n = 0, 1$, are the Hankel functions of the second kind, related to the Bessel functions of the first and second kind J_n and Y_n , respectively [56]. Note that $C(k)$ in (A10) is the well-known Theodorsen function [57]. Other defined functions are the following:

$$f_\gamma(x) \equiv \frac{4}{\pi} \frac{K[4/\varepsilon^2]}{1+\varepsilon-x} + \frac{2}{\pi} \left(1 + \frac{2}{\varepsilon} \right) \left(\frac{(1-\varepsilon+x)(1-x)}{(1+\varepsilon-x)(1+x)} \Pi \left[\frac{2}{\varepsilon} \frac{1+\varepsilon-x}{1+x}, \frac{4}{\varepsilon^2} \right] - \Pi \left[-\frac{2}{\varepsilon}, \frac{4}{\varepsilon^2} \right] \right), \quad (\text{A13})$$

$$f_{\gamma\alpha}(x) \equiv 2 \left\{ \varepsilon E \left(\frac{4}{\varepsilon^2} \right) + \frac{2(2+x) + \varepsilon(1-\varepsilon+x)}{1+\varepsilon-x} K \left(\frac{4}{\varepsilon^2} \right) + \left(1 + \frac{2}{\varepsilon} \right) (1+2x) \right. \\ \left. \times \left[\frac{(1-\varepsilon+x)(1-x)}{(1+\varepsilon-x)(1+x)} \Pi \left(\frac{2}{\varepsilon} \frac{1+\varepsilon-x}{1+x}, \frac{4}{\varepsilon^2} \right) - \Pi \left(-\frac{2}{\varepsilon}, \frac{4}{\varepsilon^2} \right) \right] \right\}, \quad (\text{A14})$$

$$f_\Gamma \equiv \frac{1}{\pi} \left[\varepsilon E \left(\frac{4}{\varepsilon^2} \right) + (2-\varepsilon) K \left(\frac{4}{\varepsilon^2} \right) \right] - 1, \quad (\text{A15})$$

$$f_{\Gamma\alpha} \equiv \varepsilon(1+\varepsilon)E \left(\frac{4}{\varepsilon^2} \right) + [6 + (3-\varepsilon)\varepsilon]K \left(\frac{4}{\varepsilon^2} \right) - 4(2+\varepsilon)\Pi \left(-\frac{2}{\varepsilon}, \frac{4}{\varepsilon^2} \right), \quad (\text{A16})$$

where $K(x)$, $E(x)$, and $\Pi(x, y)$ are the complete elliptic integral of the first kind, the complete elliptic integral of the second kind, and the incomplete elliptic integral of the third kind, respectively [58]. For the case of two airfoils in tandem configuration the integrals associated with ϖ_{12} are the following:

$$\int_{-1+\varepsilon}^{1+\varepsilon} (x-\varepsilon)^n \varpi_{12}(x, t) dx = \Gamma_{01}(t) \mathcal{I}_{\gamma, n} + \dot{\alpha}_1(t) \mathcal{I}_{\gamma\alpha, n}. \quad (\text{A17})$$

In the case of considering the first oscillating mode, some new functions appear:

$$\mathcal{R}_1(k, \varepsilon) = \int_{1-\varepsilon}^{-1} e^{-ik(\xi+\varepsilon)} \xi \sqrt{\xi^2-1} d\xi, \quad \mathcal{R}_2(k, \varepsilon) = \int_{1+\varepsilon}^{\infty} e^{-ik(\xi-\varepsilon)} \xi \sqrt{\xi^2-1} d\xi, \quad (\text{A18})$$

$$C_2(k) = \frac{H_2^{(2)}(k)}{iH_0^{(2)}(k) + H_1^{(2)}(k)}, \quad (\text{A19})$$

$$\mathcal{B}_{1\delta}(k, \varepsilon) = \frac{\mathcal{R}_2(k, \varepsilon)}{\mathbf{a}(k, \varepsilon)} - \frac{2i}{\pi} \left\{ 1 + \frac{1}{k^2} [2 + 2i(1+\varepsilon)k - (1+\varepsilon)^2 k^2] \right\} C(k), \quad (\text{A20})$$

$$\mathcal{B}_{2\delta}(k, \varepsilon) = \mathcal{Q}_\delta(k, \varepsilon)C_{1e}(k, \varepsilon) - \frac{\mathcal{R}_1(k, \varepsilon)}{\mathbf{a}(k, \varepsilon)} - \frac{i}{\pi} C_1(k), \quad (\text{A21})$$

$$\mathcal{Q}_\delta = H_2^{(2)}(k) + \frac{2}{k^2} [2ik \sin(k) - i(k^2-2) \cos(k)] \\ + \frac{ie^{i(\varepsilon-1)k}}{k^2} [(\varepsilon-1)k-1+i][(\varepsilon-1)k+1+i], \quad (\text{A22})$$

$$f_{\Gamma\delta} = 2 \int_{-1}^1 \sqrt{\frac{\xi+1-\varepsilon}{\xi-1-\varepsilon}} \xi \sqrt{1-\xi^2} d\xi, \quad (\text{A23})$$

$$\mathcal{I}_{\gamma\delta,n}(\varepsilon) = \frac{2}{\pi} \int_{-1+\varepsilon}^{1+\varepsilon} (x-\varepsilon)^n \sqrt{\frac{1+\varepsilon-x}{1-\varepsilon+x}} \int_{-1}^1 \sqrt{\frac{\xi+1-\varepsilon}{\xi-1-\varepsilon}} \frac{\xi \sqrt{1-\xi^2}}{\xi-x} d\xi dx, \quad (\text{A24})$$

and the integrals associated with ϖ_{12} are the following:

$$\int_{-1+\varepsilon}^{1+\varepsilon} (x-\varepsilon)^n \varpi_{12}(x,t) dx = \Gamma_{01}(t) \mathcal{I}_{\gamma,n} - \mathcal{V}_1(t) \mathcal{I}_{\gamma\alpha,n} - \dot{\mathcal{D}}_1(t) \mathcal{I}_{\gamma\delta,n}. \quad (\text{A25})$$

The double integral (A24) can be simplified to a single integral, integrating in x ,

$$I_{\gamma\delta} = 2 \int_{-1}^1 \left(\sqrt{(\xi-\varepsilon)^2 - 1} + \xi - \varepsilon \right) \xi \sqrt{1-\xi^2} d\xi, \quad (\text{A26})$$

$$I_{\gamma\delta,2} = 2 \int_{-1}^1 \left(\frac{1}{2} \sqrt{\frac{\xi+1-\varepsilon}{\xi-1-\varepsilon}} + (\xi-\varepsilon) \sqrt{(\xi-\varepsilon)^2 - 1} + (\xi-\varepsilon)^2 \right) \xi \sqrt{1-\xi^2} d\xi, \quad (\text{A27})$$

$$I_{\gamma\delta,3} = 2 \int_{-1}^1 \left[\sqrt{(\xi-\varepsilon)^2 - 1} \left(-\frac{1}{2} - (\xi-\varepsilon)^2 \right) - (\xi-\varepsilon)^3 \right] \xi \sqrt{1-\xi^2} d\xi. \quad (\text{A28})$$

APPENDIX B: LIFT, THRUST, MOMENT, AND FLEXURAL COEFFICIENTS FOR EACH FOIL

1. Lift coefficient

$$\mathcal{C}_L^{(i)} = \mathcal{L}_0(t) + \Gamma_{01}(t) \mathcal{L}_{01} + [\Gamma_{02}(t) + \Gamma_{12}(t)] \mathcal{L}_{02}. \quad (\text{B1})$$

Only $\mathcal{L}_0(t)$ changes when considering the flexural motion.

(a) Front foil

$$\mathcal{L}_0(t) = -\pi \left[\dot{\mathcal{U}}_1(t) + \frac{\ddot{\mathcal{D}}_1(t)}{2} \right], \quad (\text{B2})$$

$$\mathcal{L}_{01} = C_a + F_c \left[\frac{\mathcal{A}_2}{a} + \frac{2k}{\pi} (1 + \varepsilon - \sqrt{\varepsilon(\varepsilon+2)}) C_1 \right], \quad (\text{B3})$$

$$\mathcal{L}_{02} = C_b + F_a \left[\frac{\mathcal{A}_2}{a} + \frac{2k}{\pi} (1 + \varepsilon - \sqrt{\varepsilon(\varepsilon+2)}) C_1 \right]. \quad (\text{B4})$$

(b) Trailing foil

$$\mathcal{L}_0(t) = -\pi \left[\dot{\mathcal{U}}_2(t) + \frac{\ddot{\mathcal{D}}_2(t)}{2} - 2\dot{\mathcal{U}}_1(t) \mathcal{I}_{\gamma,1} - \dot{\mathcal{V}}_1(t) \left(I_{\gamma,1} + \frac{I_{\gamma\alpha,1}}{\pi} \right) - \dot{\mathcal{D}}_1(t) \left(I_{\gamma,1} + \frac{I_{\gamma\delta,1}}{\pi} \right) \right], \quad (\text{B5})$$

$$\begin{aligned} \mathcal{L}_{01} = C_c + F_a \left[-\frac{\mathcal{A}_1}{a} + \frac{2k}{\pi} (1 - \varepsilon + \sqrt{\varepsilon(\varepsilon-2)}) C_1 \right. \\ \left. + \frac{2}{\pi} \left(-i \frac{\pi k}{2} H_0^{(2)}(k) - 2 \sin(k) + 2k \cos(k) \right) C_{1e} \right], \end{aligned} \quad (\text{B6})$$

$$\begin{aligned} \mathcal{L}_{02} = C_a + F_b \left[-\frac{\mathcal{A}_1}{a} + \frac{2k}{\pi} (1 - \varepsilon + \sqrt{\varepsilon(\varepsilon-2)}) C_1 \right. \\ \left. + \frac{2}{\pi} \left(-i \frac{\pi k}{2} H_0^{(2)}(k) - 2 \sin(k) + 2k \cos(k) \right) C_{1e} \right]. \end{aligned} \quad (\text{B7})$$

2. Thrust coefficient

$$\mathcal{C}_T^{(i)} = \mathcal{E}_i \mathcal{C}_L^{(i)} + \dot{\mathcal{E}}_i \mathcal{T}_0 + \mathcal{D}_i \mathcal{T}_{\delta 1} + \dot{\mathcal{D}}_i \mathcal{T}_{\delta 2} + \Gamma_{01} \mathcal{T}_{01} + [\Gamma_{02} + \Gamma_{12}] \mathcal{T}_{02}. \quad (\text{B8})$$

(a) Front foil

$$\mathcal{T}_0 = -\pi \left(\mathcal{U}_1 + \frac{\dot{\mathcal{D}}_1}{2} \right), \quad (\text{B9})$$

$$\mathcal{T}_{\delta 1} = -\frac{\pi}{2} \dot{\mathcal{V}}_1 - \Gamma_{01} \mathcal{T}_{\delta 01} - (\Gamma_{02} + \Gamma_{12}) \mathcal{T}_{\delta 02}, \quad (\text{B10})$$

$$\mathcal{T}_{\delta 2} = -\frac{\pi}{2} \mathcal{D}_1, \quad (\text{B11})$$

$$\begin{aligned} \mathcal{T}_{01} = F_a \left\{ \left[\dot{\mathcal{D}}_1 \left(\frac{2i}{k^2} - \frac{2+ik}{k} \right) - \frac{1+ik}{k} \mathcal{V}_1 - i\mathcal{U}_1 \right] \frac{2}{\pi} F_a \mathcal{C}_1 \right. \\ \left. - \frac{1}{k} [\dot{\mathcal{D}}_1 \mathcal{C}_2 + i\mathcal{V}_1 \mathcal{C}] \right\} - F_c (\mathcal{V}_1 \mathcal{B}_1 + \dot{\mathcal{D}}_1 \mathcal{B}_{1\delta}), \end{aligned} \quad (\text{B12})$$

$$\begin{aligned} \mathcal{T}_{02} = F_b \left\{ \left[\dot{\mathcal{D}}_1 \left(\frac{2i}{k^2} - \frac{2+ik}{k} \right) - \frac{1+ik}{k} \mathcal{V}_1 - i\mathcal{U}_1 \right] \frac{2}{\pi} F_a \mathcal{C}_1 - \frac{1}{k} [\dot{\mathcal{D}}_1 \mathcal{C}_2 + i\mathcal{V}_1 \mathcal{C}] \right\} \\ - F_a (\mathcal{V}_1 \mathcal{B}_1 + \dot{\mathcal{D}}_1 \mathcal{B}_{1\delta}), \end{aligned} \quad (\text{B13})$$

where the functions $\mathcal{T}_{\delta 01}$ and $\mathcal{T}_{\delta 02}$ are given by

$$\mathcal{T}_{\delta 01} = \mathcal{C}_a - 1 + F_c \left\{ \frac{\mathcal{A}_2}{a} + \frac{2k}{\pi} [1 + 2(1 + \varepsilon)(\sqrt{\varepsilon(\varepsilon + 2)} - (1 + \varepsilon))] \mathcal{C}_1 \right\}, \quad (\text{B14})$$

$$\mathcal{T}_{\delta 02} = \mathcal{C}_b + F_a \left\{ \frac{\mathcal{A}_2}{a} + \frac{2k}{\pi} [1 + 2(1 + \varepsilon)(\sqrt{\varepsilon(\varepsilon + 2)} - (1 + \varepsilon))] \mathcal{C}_1 \right\}. \quad (\text{B15})$$

(b) Trailing foil

$$\mathcal{T}_0 = \pi \left[-\mathcal{U}_2 - \frac{\dot{\mathcal{D}}_2}{2} + 2\mathcal{U}_1 \mathcal{I}_{\gamma,1} + \mathcal{V}_1 \left(\mathcal{I}_{\gamma,1} + \frac{\mathcal{I}_{\gamma\alpha,1}}{\pi} \right) + \dot{\mathcal{D}}_1 \left(\mathcal{I}_{\gamma,1} + \frac{\mathcal{I}_{\gamma\delta,1}}{\pi} \right) \right], \quad (\text{B16})$$

$$\begin{aligned} \mathcal{T}_{\delta 1} = -\frac{\pi}{2} \dot{\mathcal{V}}_2 - 2\pi \left[\dot{\mathcal{U}}_1 (f_\Gamma - 2\mathcal{I}_{\gamma,2}) + \dot{\mathcal{V}}_1 \left(\frac{f_\Gamma}{2} + \frac{f_{\Gamma\alpha}}{2\pi} - \mathcal{I}_{\gamma,2} - \frac{\mathcal{I}_{\gamma\alpha,2}}{\pi} \right) \right. \\ \left. + \ddot{\mathcal{D}}_1 \left(\frac{f_\Gamma}{2} + \frac{f_{\Gamma\delta}}{2\pi} - \mathcal{I}_{\gamma,2} - \frac{\mathcal{I}_{\gamma\delta,2}}{\pi} \right) \right] - \Gamma_{01} \mathcal{T}_{\delta 01} - (\Gamma_{02} + \Gamma_{12}) \mathcal{T}_{\delta 02}, \end{aligned} \quad (\text{B17})$$

$$\begin{aligned} \mathcal{T}_{\delta 2} = -\pi \left[\frac{\mathcal{D}_2}{2} + \mathcal{U}_1 (f_\Gamma - 2\mathcal{I}_{\gamma,2}) + \mathcal{V}_1 \left(\frac{f_\Gamma}{2} + \frac{f_{\Gamma\alpha}}{2\pi} - \mathcal{I}_{\gamma,2} - \frac{\mathcal{I}_{\gamma\alpha,2}}{\pi} \right) \right. \\ \left. + \dot{\mathcal{D}}_1 \left(\frac{f_\Gamma}{2} + \frac{f_{\Gamma\delta}}{2\pi} - \mathcal{I}_{\gamma,2} - \frac{\mathcal{I}_{\gamma\delta,2}}{\pi} \right) \right], \end{aligned} \quad (\text{B18})$$

$$\begin{aligned} \mathcal{T}_{01} = F_c \left\{ \left[\dot{\mathcal{D}}_2 \left(\frac{2i}{k^2} - \frac{2+ik}{k} \right) - \frac{1+ik}{k} \mathcal{V}_2 - i\mathcal{U}_2 \right] \frac{2}{\pi} F_a \mathcal{C}_1 - \frac{1}{k} [\dot{\mathcal{D}}_2 \mathcal{C}_2 + i\mathcal{V}_2 \mathcal{C}] \right\} \\ - F_a (\mathcal{V}_2 \mathcal{B}_2 + \dot{\mathcal{D}}_2 \mathcal{B}_{2\delta}), \end{aligned} \quad (\text{B19})$$

$$\begin{aligned} \mathcal{T}_{02} = F_a \left\{ \left[\dot{\mathcal{D}}_2 \left(\frac{2i}{k^2} - \frac{2+ik}{k} \right) - \frac{1+ik}{k} \mathcal{V}_2 - i\mathcal{U}_2 \right] \frac{2}{\pi} F_a \mathcal{C}_1 - \frac{1}{k} [\dot{\mathcal{D}}_2 \mathcal{C}_2 + i\mathcal{V}_2 \mathcal{C}] \right\} \\ - F_b (\mathcal{V}_2 \mathcal{B}_2 + \dot{\mathcal{D}}_2 \mathcal{B}_{2\delta}), \end{aligned} \quad (\text{B20})$$

where the functions $\mathcal{T}_{\delta 01}$ and $\mathcal{T}_{\delta 01}$ are given by

$$\begin{aligned} \mathcal{T}_{\delta 01} = & \mathcal{C}_c + F_a \left\{ -\frac{\mathcal{A}_1}{\mathbf{a}} + \frac{2k}{\pi} [1 - 2(1 - \varepsilon)(\sqrt{\varepsilon(\varepsilon - 2)} + (1 - \varepsilon))] \mathcal{C}_1 \right. \\ & \left. + \frac{2k}{\pi} \left(4i \sin(k) - \frac{\pi}{2} i H_0^{(2)}(k) \right) \mathcal{C}_{1e} \right\}, \end{aligned} \quad (\text{B21})$$

$$\begin{aligned} \mathcal{T}_{\delta 02} = & \mathcal{C}_a - 1 + F_b \left\{ -\frac{\mathcal{A}_1}{\mathbf{a}} + \frac{2k}{\pi} [1 - 2(1 - \varepsilon)(\sqrt{\varepsilon(\varepsilon - 2)} + (1 - \varepsilon))] \mathcal{C}_1 \right. \\ & \left. + \frac{2k}{\pi} \left(4i \sin(k) - \frac{\pi}{2} i H_0^{(2)}(k) \right) \mathcal{C}_{1e} \right\}. \end{aligned} \quad (\text{B22})$$

3. Moment coefficient

$$\mathcal{C}_M^{(i)} = \frac{a_i}{2} \mathcal{C}_L^{(i)} + \mathcal{M}_0(t) + \Gamma_{01} \mathcal{M}_{01} + [\Gamma_{02}(t) + \Gamma_{12}(t)] \mathcal{M}_{02}. \quad (\text{B23})$$

Only $\mathcal{M}_0(t)$ changes considering the first oscillation mode.

(a) Front foil

$$\mathcal{M}_0(t) = \frac{\pi}{4} \left(\mathcal{V}_1 + \frac{\dot{\mathcal{V}}_1}{4} + \frac{\ddot{\mathcal{D}}_1}{2} \right), \quad (\text{B24})$$

$$\mathcal{M}_{01} = \frac{1}{4} \left\{ \mathcal{C}_a + F_c \left[\frac{\mathcal{A}_2}{\mathbf{a}} + \frac{2k}{\pi} \left(\frac{1}{2} + (1 + \varepsilon) \sqrt{\varepsilon(\varepsilon + 2)} - (1 + \varepsilon)^2 \right) \mathcal{C}_1 \right] \right\}, \quad (\text{B25})$$

$$\mathcal{M}_{02} = \frac{1}{4} \left\{ \mathcal{C}_b + F_a \left[\frac{\mathcal{A}_2}{\mathbf{a}} + \frac{2k}{\pi} \left(\frac{1}{2} + (1 + \varepsilon) \sqrt{\varepsilon(\varepsilon + 2)} - (1 + \varepsilon)^2 \right) \mathcal{C}_1 \right] \right\}. \quad (\text{B26})$$

(b) Trailing foil

$$\begin{aligned} \mathcal{M}_0(t) = & \frac{\pi}{4} \left(\mathcal{V}_2 + \frac{\dot{\mathcal{V}}_2}{4} + \frac{\ddot{\mathcal{D}}_2}{2} \right) \\ & + \frac{1}{2} \left[-\Gamma_{01} \left(\mathcal{I}_{\gamma,1} + \frac{f_{\Gamma}}{2} \right) + \mathcal{B}_1 \left(\mathcal{I}_{\gamma\alpha,1} + \frac{f_{\Gamma\alpha}}{2} \right) + \dot{\mathcal{D}}_1 \left(\mathcal{I}_{\gamma\delta,1} + \frac{f_{\Gamma\delta}}{2} \right) \right] \\ & + \frac{1}{4} \left[\dot{\Gamma}_{01} \left(\mathcal{I}_{\gamma,2} - \frac{f_{\Gamma}}{2} \right) - \dot{\mathcal{B}}_1 \left(\mathcal{I}_{\gamma\alpha,2} - \frac{f_{\Gamma\alpha}}{2} \right) - \ddot{\mathcal{D}}_1 \left(\mathcal{I}_{\gamma\delta,2} - \frac{f_{\Gamma\delta}}{2} \right) \right], \end{aligned} \quad (\text{B27})$$

$$\begin{aligned} \mathcal{M}_{01} = & \frac{1}{4} \left\{ \mathcal{C}_c + F_a \left[-\frac{\mathcal{A}_1}{\mathbf{a}} + \frac{2k}{\pi} \left(\frac{1}{2} - (1 - \varepsilon) \sqrt{\varepsilon(\varepsilon - 2)} - (1 - \varepsilon)^2 \right) \mathcal{C}_1 \right. \right. \\ & \left. \left. + \frac{2k}{\pi} \left(2i \sin(k) - i \frac{\pi}{2} H_0^{(2)}(k) \right) \mathcal{C}_{1e} \right] \right\}, \end{aligned} \quad (\text{B28})$$

$$\begin{aligned} \mathcal{M}_{02} = & \frac{1}{4} \left\{ \mathcal{C}_a + F_b \left[-\frac{\mathcal{A}_1}{\mathbf{a}} + \frac{2k}{\pi} \left(\frac{1}{2} - (1 - \varepsilon) \sqrt{\varepsilon(\varepsilon - 2)} - (1 - \varepsilon)^2 \right) \mathcal{C}_1 \right. \right. \\ & \left. \left. + \frac{2k}{\pi} \left(2i \sin(k) - i \frac{\pi}{2} H_0^{(2)}(k) \right) \mathcal{C}_{1e} \right] \right\}. \end{aligned} \quad (\text{B29})$$

4. Flexural coefficient

$$\mathcal{C}_F^{(i)} = p [4\mathcal{C}_{Mp}^{(i)} - p\mathcal{C}_L^{(i)}] + \mathcal{F}_0(t) + \Gamma_{01}(t) \mathcal{F}_{01} + [\Gamma_{02}(t) + \Gamma_{12}(t)] \mathcal{F}_{02}. \quad (\text{B30})$$

(a) Front foil

$$F_0(t) = -\frac{\pi}{4} \left[\dot{\mathcal{U}}_1 - \mathcal{V}_1 + \frac{\ddot{D}_1}{3} \right], \quad (\text{B31})$$

$$F_{01} = \frac{1}{2} \left\{ \mathcal{C}_a + \frac{\mathcal{A}_2}{\mathbf{a}} F_c + \frac{2}{3} \left[(1 + \varepsilon)^3 - \left((1 + \varepsilon)^2 + \frac{1}{2} \right) \sqrt{\varepsilon(\varepsilon + 2)} \right] \frac{2k}{\pi} C_{1e} F_c \right\}, \quad (\text{B32})$$

$$F_{02} = \frac{1}{2} \left\{ \mathcal{C}_b + \frac{\mathcal{A}_2}{\mathbf{a}} F_a + \frac{2}{3} \left[(1 + \varepsilon)^3 - \left((1 + \varepsilon)^2 + \frac{1}{2} \right) \sqrt{\varepsilon(\varepsilon + 2)} \right] \frac{2k}{\pi} C_{1e} F_a \right\}. \quad (\text{B33})$$

(b) Trailing foil

$$F_0(t) = -\frac{\pi}{4} \left[\dot{\mathcal{U}}_2 - \mathcal{V}_2 + \frac{\ddot{D}_2}{3} \right] - \mathcal{V}_1 \mathcal{I}_{\gamma\alpha,2} - \dot{D}_1 \mathcal{I}_{\gamma\delta,2} + \frac{\pi}{3} \left[2\dot{\mathcal{U}}_1 \mathcal{I}_{\gamma,3} + \dot{\mathcal{V}}_1 \left(\mathcal{I}_{\gamma,3} + \frac{\mathcal{I}_{\gamma,3}}{\pi} \right) \right], \quad (\text{B34})$$

$$F_{01} = \frac{1}{2} \left\{ \mathcal{C}_c - \frac{\mathcal{A}_1}{\mathbf{a}} F_a - \left(ikH_0^{(2)}(k) - \frac{8k}{3\pi} \cos(k) \right) C_{1e} F_a \right. \\ \left. + \frac{2}{3} \left[(1 - \varepsilon)^3 + \left((1 - \varepsilon)^2 + \frac{1}{2} \right) \sqrt{\varepsilon(\varepsilon - 2)} \right] \frac{2k}{\pi} C_{1e} F_a \right\}, \quad (\text{B35})$$

$$F_{02} = \frac{1}{2} \left\{ \mathcal{C}_a - \frac{\mathcal{A}_1}{\mathbf{a}} F_b - \left(ikH_0^{(2)}(k) - \frac{8k}{3\pi} \cos(k) \right) C_{1e} F_b \right. \\ \left. + \frac{2}{3} \left[(1 - \varepsilon)^3 + \left((1 - \varepsilon)^2 + \frac{1}{2} \right) \sqrt{\varepsilon(\varepsilon - 2)} \right] \frac{2k}{\pi} C_{1e} F_b \right\}. \quad (\text{B36})$$

-
- [1] D. E. Alexander, Unusual phase relationships between the forewings and hindwings in flying dragonflies, *J. Exp. Biol.* **109**, 379 (1984).
- [2] A. Azuma and T. Watanabe, Flight performance of a dragonfly, *J. Exp. Biol.* **137**, 221 (1988).
- [3] A. L. R. Thomas, G. K. Taylor, R. B. Srygley, R. L. Nudds, and R. J. Bomphrey, Dragonfly flight: Free-flight and tethered flow visualizations reveal a diverse array of unsteady lift-generating mechanisms, controlled primarily via angle of attack, *J. Exp. Biol.* **207**, 4299 (2004).
- [4] I. Akhtar, R. Mittal, G. V. Lauder, and E. Drucker, Hydrodynamics of biologically inspired tandem flapping foil configuration, *Theor. Comput. Fluid Dyn.* **21**, 155 (2007).
- [5] G. Liu, Y. Ren, H. Dong, O. Akanyeti, J. C. Liao, and G. V. Lauder, Computational analysis of vortex dynamics and performance enhancement due to body-fin and fin-fin interactions in fish-like locomotion, *J. Fluid Mech.* **829**, 65 (2017).
- [6] D. Weihs, Hydromechanics of fish schooling, *Nature (London)* **241**, 290 (1973).
- [7] I. L. Bajec and F. H. Heppner, Organized flight in birds, *Anim. Behav.* **78**, 777 (2009).
- [8] L. E. Muscutt, G. Dyke, G. D. Weymouth, D. Naish, C. Palmer, and B. Ganapathisubramani, The four-flipper swimming method of plesiosaurs enabled efficient and effective locomotion, *Proc. R. Soc. London, Ser. B* **284**, 20170951 (2017).
- [9] I. H. Tuncer and M. F. Platzer, Thrust generation due to airfoil flapping, *AIAA J.* **34**, 324 (1996).
- [10] S. L. Lan and M. Sun, Aerodynamic interactions of two airfoils in unsteady motion, *Acta Mech.* **150**, 39 (2001).
- [11] T. M. Broering and Y. Liang, Numerical study of tandem flapping wing aerodynamics in both two and three dimensions, *Comput. Fluids* **115**, 124 (2015).
- [12] K. B. Lua, H. Lu, X. H. Zhang, T. T. Lim, and K. S. Yeo, Aerodynamics of two-dimensional flapping wings in tandem configuration, *Phys. Fluids* **28**, 121901 (2016).

- [13] J. Ortega-Casanova and R. Fernandez-Feria, Analysis of the aerodynamic interaction between two plunging plates in tandem at low Reynolds number for maximum propulsive efficiency, *J. Fluids Struct.* **63**, 351 (2016).
- [14] L. E. Muscutt, G. D. Weymouth, and B. Ganapathisubramani, Performance augmentation mechanism of in-line tandem flapping foils, *J. Fluid Mech.* **827**, 484 (2017).
- [15] X. Lin, J. Wu, T. Zhang, and L. Yang, Phase difference effect on collective locomotion of two tandem autopropelled flapping foils, *Phys. Rev. Fluids* **4**, 054101 (2019).
- [16] J. Ortega-Casanova and R. Fernandez-Feria, maximum propulsive efficiency of two pitching and plunging plates in tandem at low Reynolds number, *Int. J. Numer. Methods Heat Fluid Flow* **29**, 4013 (2019).
- [17] G. Arranz, O. Flores, and M. Garcia-Villalba, Three-dimensional effects on the aerodynamic performance of flapping wings in tandem configuration, *J. Fluids Struct.* **94**, 102893 (2020).
- [18] K. D. Jones and M. F. Platzer, An experimental and numerical investigation of flapping-wing propulsion, AIAA Paper 99-0995 (1999).
- [19] J. Warkentin and J. DeLaurier, Experimental aerodynamic study of tandem flapping membrane wings, *J. Aircraft* **44**, 1653 (2007).
- [20] F. O. Lehmann, Wing-wake interaction reduces power consumption in insect tandem wings, *Exp. Fluids* **46**, 765 (2009).
- [21] B. M. Boschitsch, P. A. Dewey, and A. J. Smits, Propulsive performance of unsteady tandem hydrofoils in an in-line configuration, *Phys. Fluids* **26**, 051901 (2014).
- [22] Y. Zheng, Y. Wu, and H. Tang, An experimental study on the forewing-hindwing interactions in hovering and forward flights, *Int. J. Heat Fluid Flow* **59**, 62 (2016).
- [23] S. Ramanarivo, F. Fang, A. Oza, J. Zhang, and L. Ristroph, Flow interactions lead to orderly formations of flapping wings in forward flight, *Phys. Rev. Fluids* **1**, 071201 (2016).
- [24] M. Kurt and K. W. Moored, Flow interactions of two- and three-dimensional networked bio-inspired control elements in an in-line arrangement, *Bioinspir. Biomim.* **13**, 045002 (2018).
- [25] F. J. Huera-Huarte, Propulsive performance of a pair of pitching foils in staggered configurations, *J. Fluids Struct.* **81**, 1 (2018).
- [26] J. W. Newbolt, J. Zhang, and L. Ristroph, Flow interactions between uncoordinated flapping swimmers give rise to group cohesion, *Proc. Natl. Acad. Sci. USA* **116**, 2419 (2019).
- [27] H. Nagai, K. Fujita, and M. Murozono, Experimental study on forewing-hindwing phasing in hovering and forward flapping flight, *AIAA J.* **57**, 3779 (2019).
- [28] H. Bosch, Interfering airfoils in two-dimensional unsteady, incompressible flow, Technical Report CP-227, AGARD (1978).
- [29] C. E. Lan, The unsteady quasi-vortex-lattice method with applications to animal propulsion, *J. Fluid Mech.* **93**, 747 (1979).
- [30] J. Alaminos-Quesada and R. Fernandez-Feria, Aerodynamics of heaving and pitching foils in tandem from linear potential theory, *AIAA J.* **58**, 37 (2020).
- [31] W. Schmidt, Der Wellpropeller, ein neuer Antrieb für Wasser-, Land-, und Luftfahrzeuge, *Z. Flugwiss* **13**, 472 (1965).
- [32] J. R. Usherwood and F. O. Lehmann, Phasing of dragonfly wings can improve aerodynamic efficiency by removing swirl, *J. R. Soc. Interface* **5**, 1303 (2008).
- [33] R. Fernandez-Feria, Linearized propulsion theory of flapping airfoils revisited, *Phys. Rev. Fluids* **1**, 084502 (2016).
- [34] S. Heathcote, D. Martin, and I. Gursul, Flexible flapping airfoil propulsion at zero freestream velocity, *AIAA J.* **42**, 2196 (2004).
- [35] S. Heathcote and I. Gursul, Flexible flapping airfoil propulsion at low Reynolds numbers, *AIAA J.* **45**, 1066 (2007).
- [36] T. Y. Wu, Fish swimming and bird/insect flight, *Annu. Rev. Fluid Mech.* **43**, 25 (2011).
- [37] D. B. Quinn, G. V. Lauder, and A. J. Smits, Maximizing the efficiency of a flexible propulsor using experimental optimization, *J. Fluid Mech.* **767**, 430 (2015).
- [38] M. Olivier and G. Dumas, A parametric investigation of the propulsion of 2D chordwise-flexible flapping wings at low Reynolds number using numerical simulations, *J. Fluids Struct.* **63**, 210 (2016).

- [39] S. Wang and L. J. Zhang, Self-propulsion of flapping bodies in viscous fluids: Recent advances and perspectives, *Acta Mech. Sin.* **32**, 980 (2016).
- [40] A. J. Smits, Undulatory and oscillatory swimming, *J. Fluid Mech.* **874**, P1 (2019).
- [41] S. Alben, Wake-mediated synchronization and drafting in coupled flags, *J. Fluid Mech.* **641**, 489 (2009).
- [42] A. P. Maertens, A. Gao, and M. S. Triantafyllou, Optimal undulatory swimming for a single fish-like body and for a pair of interacting swimmers, *J. Fluid Mech.* **813**, 301 (2017).
- [43] S. G. Park and H. J. Sung, Hydrodynamics of flexible fins propelled in tandem, diagonal, triangular and diamond configurations, *J. Fluid Mech.* **840**, 154 (2018).
- [44] L. Cong, B. Teng, and L. Cheng, Hydrodynamic behavior of two-dimensional tandem-arranged flapping flexible foils in uniform flow, *Phys. Fluids* **32**, 021903 (2020).
- [45] J. Ryu, J. Yang, S. G. Park, and H. J. Sung, Phase-mediated locomotion of two self-propelled flexible plates in a tandem arrangement, *Phys. Fluids* **32**, 041901 (2020).
- [46] J. Alaminos-Quesada and R. Fernandez-Feria, Propulsion of a foil undergoing a flapping undulatory motion from the impulse theory in the linear potential limit, *J. Fluid Mech.* **883** A19 (2020).
- [47] See Supplemental Material at <http://link.aps.org/supplemental/10.1103/PhysRevFluids.6.013102> for the explicit expressions of the different functions in the cycle-averaged coefficients.
- [48] Th. von Kármán and W. R. Sears, Airfoil theory for non-uniform motion, *J. Aeronaut. Sci.* **5**, 379 (1938).
- [49] J. C. Wu, Theory for the aerodynamic force and moment in viscous flows, *AIAA J.* **19**, 432 (1981).
- [50] R. Fernandez-Feria, Note on optimum propulsion of heaving and pitching airfoils from linear potential theory, *J. Fluid Mech.* **826**, 781 (2017).
- [51] A. Martín-Alcántara and R. Fernandez-Feria, Assessment of two vortex formulations for computing forces of a flapping foil at high Reynolds numbers, *Phys. Rev. Fluids* **4**, 024702 (2019).
- [52] R. Fernandez-Feria and E. Sanmiguel-Rojas, Comparison of aerodynamic models for two-dimensional pitching foils with experimental data, *Phys. Fluids* **31**, 057104 (2019).
- [53] D. Asselin and C. H. K. Williamson, Addition of Passive dynamics to a heaving airfoil to improve performance, in *Fluid-Structure Interactions Employing Cyber-Physical Fluid Dynamics*, Technical Report AFRL-AFOSR-VA-TR-2019-0114 (Air Force Research Laboratory, 2019).
- [54] Th. von Kármán and J. M. Burgers, General aerodynamic theory - Perfect fluids, in *Aerodynamic Theory*, edited by W. F. Durand (Springer, Berlin, 1935).
- [55] I. E. Garrick, *Propulsion of a Flapping and Oscillating Airfoil*, Technical Report TR 567 (NACA, 1936).
- [56] F. W. J. Olver and L. C. Maximon, Bessel functions, in *NIST Handbook of Mathematical Functions*, edited by F. W. J. Olver, D. W. Lozier, R. F. Boisvert, and C. W. Clark (Cambridge University Press, Cambridge, 2010), pp. 215–286.
- [57] T. Theodorsen, *General Theory of Aerodynamic Instability and the Mechanism of Flutter*, Technical Report TR 496 (NACA, 1935).
- [58] M. Abramowitz and I. A. Stegun, *Handbook of Mathematical Functions* (Dover, New York, 1965).